LETTER

doi:10.1038/nature17183

Bidirectional electromagnetic control of the hypothalamus regulates feeding and metabolism

Sarah A. Stanley[1], Leah Kelly[1], Kaamashri N. Latcha[1], Sarah F. Schmidt[1], Xiaofei Yu[1], Alexander R. Nectow[1], Jeremy Sauer[2], Jonathan P. Dyke[3], Jonathan S. Dordick[2] & Jeffrey M. Friedman[1,4]

Targeted, temporally regulated neural modulation is invaluable in determining the physiological roles of specific neural populations or circuits. Here we describe a system for non-invasive, temporal activation or inhibition of neuronal activity *in vivo* and its use to study central nervous system control of glucose homeostasis and feeding in mice. We are able to induce neuronal activation remotely using radio waves or magnetic fields via Cre-dependent expression of a GFP-tagged ferritin fusion protein tethered to the cation-conducting transient receptor potential vanilloid 1 (TRPV1) by a camelid anti-GFP antibody (anti-GFP–TRPV1)[1]. Neuronal inhibition via the same stimuli is achieved by mutating the TRPV1 pore, rendering the channel chloride-permeable. These constructs were targeted to glucose-sensing neurons in the ventromedial hypothalamus in glucokinase–Cre mice, which express Cre in glucose-sensing neurons[2]. Acute activation of glucose-sensing neurons in this region increases plasma glucose and glucagon, lowers insulin levels and stimulates feeding, while inhibition reduces blood glucose, raises insulin levels and suppresses feeding. These results suggest that pancreatic hormones function as an effector mechanism of central nervous system circuits controlling blood glucose and behaviour. The method we employ obviates the need for permanent implants and could potentially be applied to study other neural processes or used to regulate other, even dispersed, cell types.

While electrode stimulation and lesioning studies suggest that hypothalamic neurons regulate blood glucose and feeding[3], these methods affect both cells and fibres of passage[4–6] and do not define contributing cell types[7]. Previously we showed that radio waves or magnetic fields can control calcium (Ca^{2+}) entry and gene expression using ferritin nanoparticles tethered to the temperature-sensitive TRPV1 channel[1]. In this report, we tested the utility of our approach for neural activation and investigate the function of hypothalamic glucose-sensing neurons. A replication-deficient adenovirus with Cre-dependent expression of anti-GFP–TRPV1/GFP–ferritin (Ad-FLEX-anti-GFP-TRPV1/GFP-ferritin) was injected unilaterally into the ventromedial hypothalamus (VMH) of glucokinase–Cre (GK–Cre) mice, which express Cre in glucose-sensing neurons[2] (Extended Data Fig. 1a), targeting ~2,000 neurons (see Methods), similar to previous studies[8,9]. Radio frequency (RF) treatment (465 kHz) of these mice significantly increased blood glucose (change in blood glucose at 30 min: RF-treated, $48.9 \pm 16.9\,mg\,dl^{-1}$ versus untreated, $-0.7 \pm 12.9\,mg\,dl^{-1}$; $P < 0.05$; at 45 min: RF-treated, $91.3 \pm 28.2\,mg\,dl^{-1}$ versus untreated, $8.7 \pm 11.1\,mg\,dl^{-1}$; $P < 0.05$) and the cumulative change in blood glucose (area under the curve (AUC; 0–90 min): RF-treated, $5{,}562 \pm 1{,}977\,mg\,dl^{-1}$ min versus untreated, $62 \pm 1{,}184\,mg\,dl^{-1}$ min; $P < 0.05$) (Fig. 1b, c). The time course and extent of glucose changes after RF treatment were almost superimposable with those after optogenetic activation of VMH GK–Cre neurons, albeit with a slight delay (Fig. 1b, c). RF treatment of GK–Cre mice with VMH injection of anti-GFP–TRPV1/GFP–ferritin halved plasma insulin, increased plasma glucagon threefold and significantly induced expression of the hepatic gluconeogenic enzyme[10], glucose-6-phosphatase (Fig. 1d). Thus, remote activation of glucose-sensing neurons regulated pancreatic hormones to increase blood glucose. Blood glucose changes were dependent on RF field strength and duration (Extended Data Fig. 2a–d). RF treatment did not alter blood glucose in wild-type mice with VMH injection of anti-GFP–TRPV1/GFP–ferritin (Extended Data Fig. 3). RF treatment induced c-Fos expression only in GFP-expressing neurons and not in RF-treated wild-type mice (Extended Data Fig. 1d). Anti-GFP–TRPV1/GFP–ferritin expression, with or without RF, did not alter apoptotic cell count compared to control virus expressing GFP (Extended Data Fig. 1d, e).

Consistent with these *in vivo* data, RF significantly increased the number of cells with raised intracellular Ca^{2+} in a hypothalamic N38 cell line stably expressing anti-GFP–TRPV1/GFP–ferritin. These effects were blocked by the TRP channel inhibitor ruthenium red. The mode response time was 11–15 s after RF onset (Extended Data Fig. 4a–c). Calcium responses were proportional to RF field strength and a 10 s pulse significantly increased intracellular Ca^{2+} (Extended Data Fig. 4d–g). RF treatment of N38 cells expressing anti-GFP–TRPV1/GFP–ferritin also significantly increased targets of Ca^{2+} signalling, phosphorylated-cAMP-response element-binding protein (pCREB)[11] and c-Fos[12], and these effects were blocked by ruthenium red (Extended Data Fig. 4h, i). RF treatment of N38 cells without anti-GFP–TRPV1/GFP–ferritin induced a small increase in c-Fos and no increase in pCREB (Extended Data Fig. 6). Immunohistochemistry, electron microscopy and immuno-electron microscopy confirmed co-expression and co-localization of anti-GFP–TRPV1 and GFP–ferritin *in vitro* (Extended Data Fig. 5).

Non-invasive neural inhibition would provide a valuable research tool and potentially offer an alternative to deep brain stimulation which may act by neural inhibition[13]. An amino acid substitution, from isoleucine to lysine in the S6 pore region of TRPM2 and M8 changed ionic selectivity from cations to chloride (Cl^-) ions[14]. We introduced and tested an analogous mutation in TRPV1 S6 region (I679K) (Fig. 2a) to create the $TRPV1^{mutant}$ channel. In N38 cells stably expressing anti-GFP–$TRPV1^{mutant}$/GFP–ferritin, the TRP agonist 2-aminoethoxydiphenyl borate (2-APB) significantly increased intracellular Cl^- levels measured by MQAE quenching. This effect was blocked by ruthenium red (Fig. 2b and Extended Data Fig. 8). RF treatment of N38 cells expressing anti-GFP–$TRPV1^{mutant}$/GFP–ferritin significantly reduced pCREB levels and failed to increase c-Fos expression (Extended Data Fig. 7a).

We next tested whether remote inhibition of hypothalamic glucose-sensing neurons altered glucose metabolism *in vivo*. RF treatment of fasted GK–Cre mice following VMH injection of adenovirus with Cre-dependent expression of anti-GFP–$TRPV1^{mutant}$/GFP–ferritin (Ad-FLEX-anti-GFP-$TRPV1^{mutant}$/GFP-ferritin) significantly

[1]Laboratory of Molecular Genetics, Rockefeller University, New York, New York 10065, USA. [2]Department of Chemical & Biological Engineering, Center for Biotechnology & Interdisciplinary Studies, Rensselaer Polytechnic Institute, Troy, New York 12180, USA. [3]Department of Radiology, Weill Cornell Medical College, New York, New York 10065, USA. [4]Howard Hughes Medical Institute, New York, New York 10065, USA.

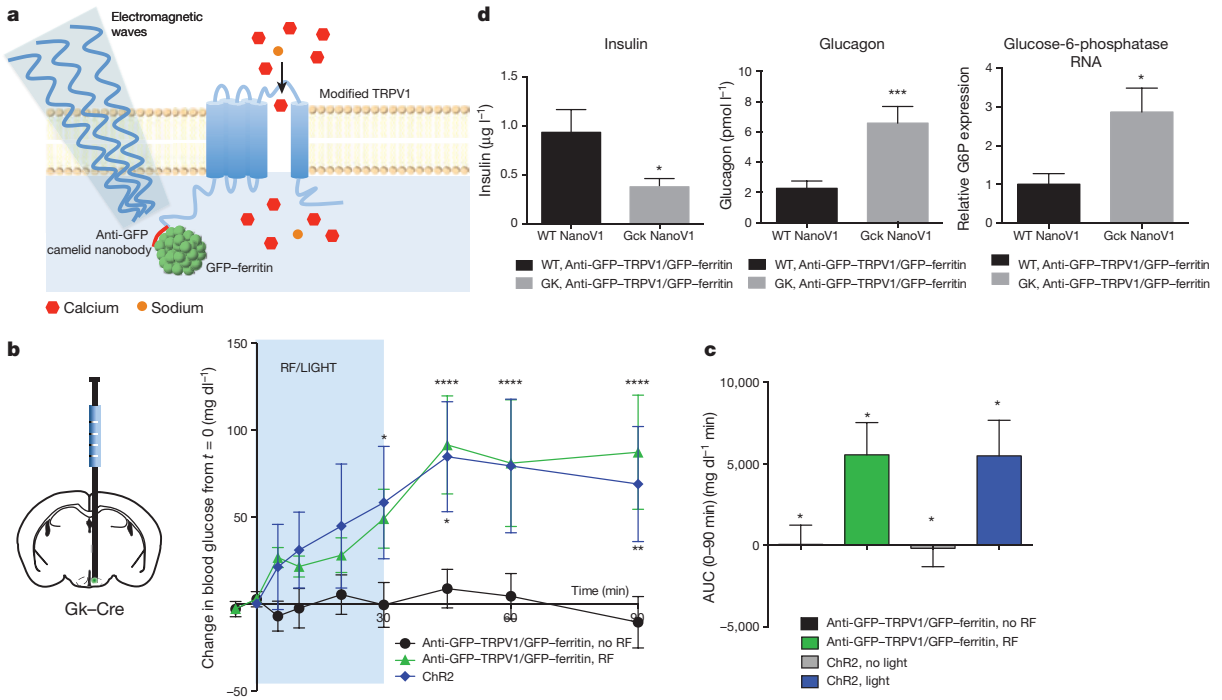

Figure 1 | Remote neural activation *in vivo* using radio waves. a, Schema of activation system. **b**, **c**, Change in blood glucose (**b**) and cumulative blood glucose (**c**) with RF treatment of GK–Cre mice (VMH injection Ad-FLEX-anti-GFP-TRPV1/GFP-ferritin, $n = 13$; VMH injection rAAV-FLEX-ChR2, $n = 4$). Values are mean ± s.e.m.; two-way ANOVA with Sidak's multiple comparison test; $^{*}P < 0.05$, $^{**}P < 0.01$, $^{****}P < 0.0001$. ChR2, channelrhodopsin 2. **d**, RF treatment of GK–Cre (GK) or wild-type (WT) mice with VMH Ad-FLEX-anti-GFP-TRPV1/GFP-ferritin on plasma insulin (GK–Cre, $n = 8$; wild type, $n = 8$), glucagon (GK–Cre, $n = 6$; wild type, $n = 11$) and hepatic glucose-6-phosphatase expression (GK–Cre, $n = 12$; wild type, $n = 9$).Values are mean ± s.e.m.; two-tailed, unpaired Student's *t*-test or Mann–Whitney *U*-test; $^{*}P < 0.05$, $^{***}P < 0.005$. WT nanoV1 refers to wild-type mice with VMH injection of Ad-FLEX-anti-GFP-TRPV1/GFP-ferritin, Gck NanoV1 indicates GK-Cre mice with VMH injection of Ad-FLEX-anti-GFP-TRPV1/GFP-ferritin.

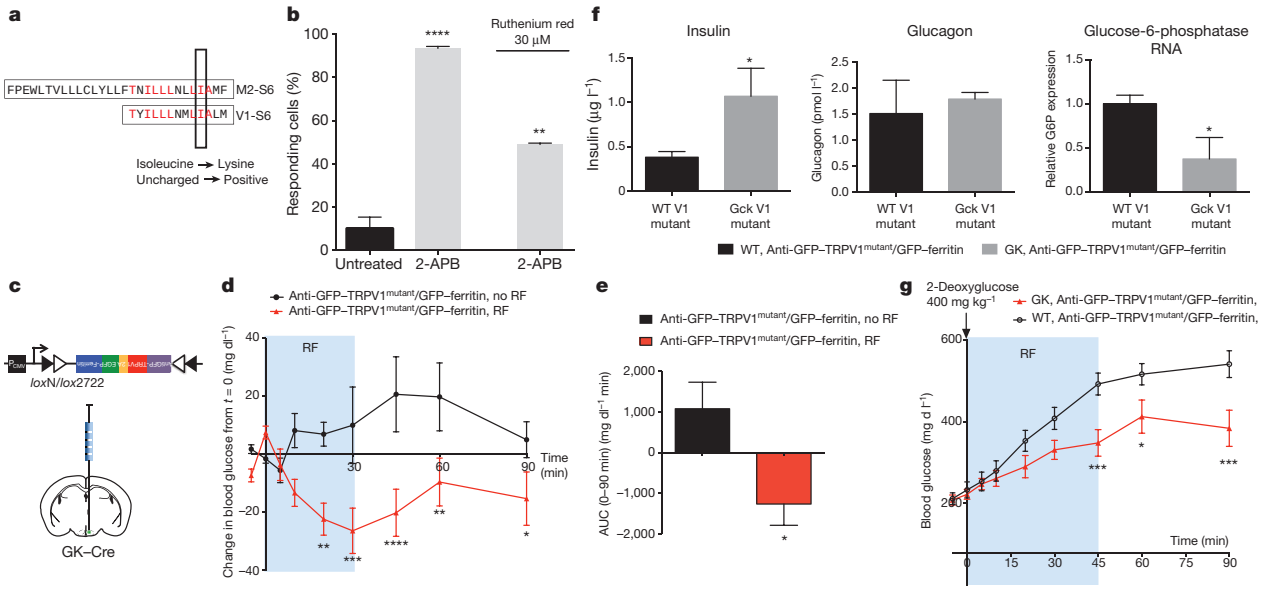

Figure 2 | Remote neural inhibition *in vitro* and *in vivo* using radio waves. a, Amino acid sequences for TRPM2 and TPRV1 S6 regions indicating substitution site. **b**, Responding cells (>10% decrease in MQAE (*N*-(ethoxycarbonylmethyl)-6-methoxyquinolinium bromide) fluorescence) with 2-APB (4 replicates, 20 cells) alone or with ruthenium red (2 replicates, 6 cells). Values are mean ± s.e.m. Kruskal–Wallis with Dunn's multiple comparison test; $^{**}P < 0.01$, $^{****}P < 0.001$ versus untreated. **c**, Construct for Cre-dependent expression of anti-GFP–TRPV1^{mutant}/GFP–ferritin. **d**, **e**, Change in blood glucose (**d**) and cumulative blood glucose (**e**) with RF treatment of GK–Cre mice with VMH injection of Ad-FLEX-anti-GFP-TRPV1^{mutant}/GFP-ferritin ($n = 13$).Values are mean ± s.e.m.; two-way ANOVA with Sidak's multiple comparison test and two-tailed Student's *t*-test; $^{*}P < 0.05$, $^{**}P < 0.01$, $^{***}P < 0.001$, $^{****}P < 0.0001$. **f**, RF treatment of GK–Cre (GK) or wild-type (WT) mice with VMH injection of Ad-FLEX-anti-GFP-TRPV1^{mutant}/GFP-ferritin on plasma insulin (GK–Cre, $n = 9$; wild type, $n = 9$), glucagon (GK–Cre, $n = 5$; wild type, $n = 9$) and hepatic glucose-6-phosphatase expression (GK–Cre, $n = 4$; wild type, $n = 8$).Values are mean ± s.e.m.; two-tailed, unpaired Student's *t*-test; $^{*}P < 0.05$. **g**, RF treatment of GK–Cre ($n = 6$) or wild-type ($n = 9$) mice with VMH injection of Ad-FLEX-anti-GFP-TRPV1^{mutant}/GFP-ferritin on blood glucose with 2-deoxyglucose treatment. Values are mean ± s.e.m.; two-way ANOVA with Sidak's multiple comparison test; $^{*}P < 0.05$, $^{***}P < 0.001$.

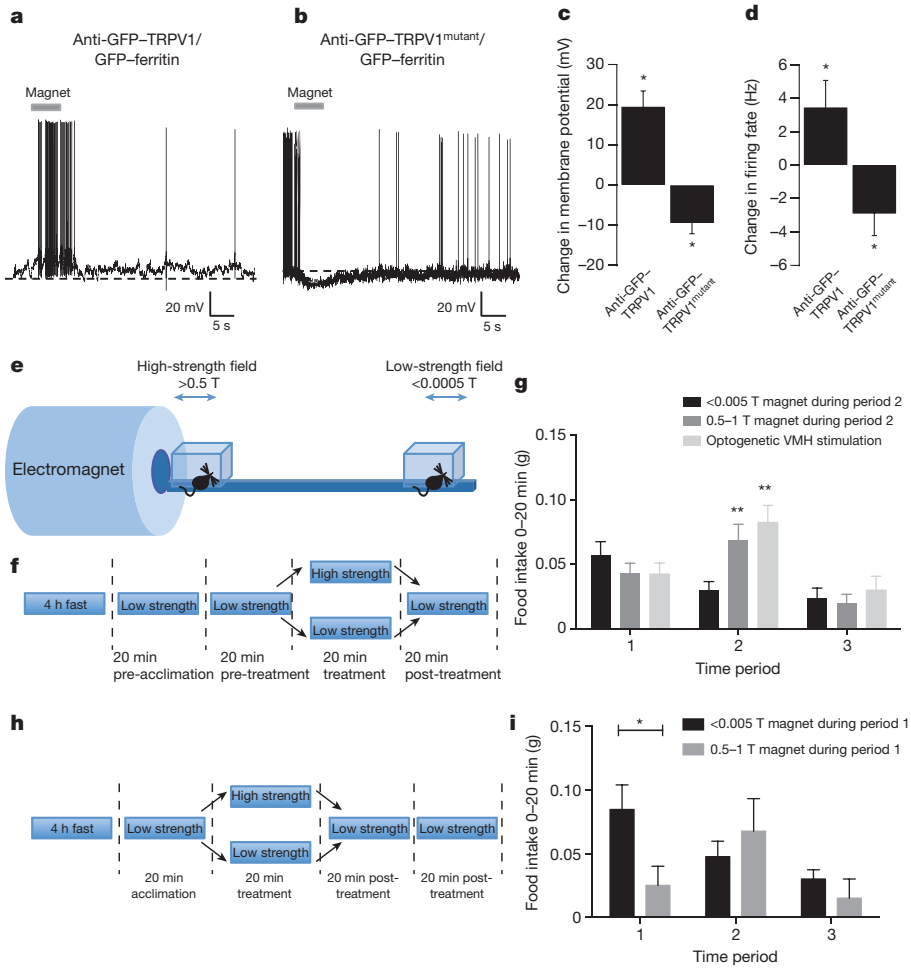

Figure 3 | Remote neural modulation *in vitro* and *in vivo* using magnetic field. a, **b**, Representative whole-cell current-clamp trace with magnet treatment (5 s) from GK–Cre VMH neurons in *ex vivo* slices expressing (**a**) anti-GFP-TRPV1/GFP-ferritin and (**b**) anti-GFP-TRPV1^{Mutant}/GFP-ferritin (of 14 and 6 recordings, respectively). **c**, **d**, Magnet treatment on membrane potential (**c**) and firing rate (**d**) in VMH neurons expressing anti-GFP–TRPV1/GFP–ferritin ($n = 14$ and 16 cells, respectively) and anti-GFP–TRPV1^{mutant}/GFP–ferritin ($n = 6$ and 6 cells, respectively). Values are mean ± s.e.m.; Wilcoxon matched pairs. **e**, **f**, Schema (**e**) and protocol (**f**) for magnetic field neural activation to examine food intake. **g**, Food intake with magnet treatment in GK–Cre mice (VMH injection of Ad-FLEX-anti-GFP-TRPV1/GFP-ferritin, $n = 6$; VMH injection of rAAV-FLEX-ChR2, $n = 4$). No replicates.Values are mean ± s.e.m.; two-way ANOVA with Sidak's multiple comparisons; $^{**}P < 0.01$. **h**, Protocol for magnetic field neural inhibition to examine food intake. **i**, Food intake with magnet treatment in GK–Cre mice with VMH injection of Ad-FLEX-anti-GFP-TRPV1^{mutant}/GFP-ferritin ($n = 6$). No replicates.Values are mean ± s.e.m.; two-way ANOVA with Sidak's multiple comparisons; $^{*}P < 0.05$.

reduced blood glucose (change in blood glucose at 20 min: RF-treated, -22.5 ± 5.5 mg dl^{-1} versus untreated, 6.8 ± 4.1 mg dl^{-1}; $P < 0.01$; at 30 min: RF-treated, -26.5 ± 7.8 mg dl^{-1} versus untreated, 9.9 ± 13.1 mg dl^{-1}; $P < 0.00^{1}$; at 45 min: RF-treated, -20.3 ± 8.2 mg dl^{-1} versus untreated, 20.6 ± 12.9 mg dl^{-1}; $P < 0.0001$) and the cumulative change in blood glucose (Fig. 2c–e). RF treatment of these mice significantly increased insulin without a rise in glucagon and significantly reduced hepatic glucose-6-phosphatase expression (Fig. 2f). Inhibition of these neurons also blunted the hyperglycaemic response to 2-deoxyglucose, a non-metabolizable form of glucose that mimics hypoglycemia[15] (Fig. 2g and Extended Data Fig. 7c). RF treatment did not affect wild-type mice with VMH injection of anti-GFP–TRPV1^{mutant}/GFP–ferritin (Extended Data Fig. 7d). These results suggest that hypothalamic glucose-sensing neurons are necessary for the normal counter-regulatory response to hypoglycaemia and to maintain blood glucose after an overnight fast.

We previously showed that ferritin's superparamagnetic properties allow ferritin-tethered TRPV1 to activate gene expression in a magnetic field[1,16]. We next tested whether a magnetic field could modulate neural activity. We were unable to make electrophysiological recordings using radio waves because of electrode heating and recording artefacts. Magnet treatment (5 s) induced a significant inward current in HEK or N38 cells expressing anti-GFP–TRPV1/GFP–ferritin and an outward current in HEK or N38 cells expressing TRPV1^{mutant}/GFP–ferritin (Extended Data Fig. 8a–f). Peak magnet-induced current displayed a rise time of 0.62 ± 0.4 s and a 37% decay time of 1.1 ± 0.74 s for anti-GFP–TRPV1/GFP–ferritin and 2.29 ± 1.8 s and 11.7 ± 4.9 s respectively for anti-GFP–TRPV1^{mutant}/GFP–ferritin. The current–voltage relationship of TRPV1^{mutant} with different intracellular anions (Extended Data Fig. 8i, j) was consistent with analogous pore loop mutations in TRPM2 and TRPM8[14]. Magnet treatment increased intracellular calcium in N38 cells expressing anti-GFP–TRPV1/GFP–ferritin and intracellular chloride in N38 cells expressing anti-GFP–TRPV1^{mutant}/GFP–ferritin. These effects were blocked by ruthenium red (Extended Data Fig. 8k–o).

We next tested the effects of magnet treatment on neural activity *ex vivo* in slices from GK–Cre mice crossed to the reporter strain *Rosa-lox-stop-lox-tdTomato* after VMH injection of Ad-anti-GFP-TRPV1/GFP-ferritin or Ad-anti-GFP-TRPV1^{mutant}/GFP-ferritin. In slices from mice injected with Ad-anti-GFP-TRPV1/GFP-ferritin, magnet treatment (5 s) depolarized neurons expressing tdTomato and GFP, significantly increasing membrane potential (16.39 ± 2.9 mV, $P < 0.001$) and firing rate (2.355 ± 0.63 Hz, $P < 0.001$) in 76% of neurons. Magnet treatment

(5 s) of slices from mice injected with Ad-anti-GFP-TRPV1^{mutant}/GFP-ferritin significantly hyperpolarized neurons by 4.7 ± 1.1 mV ($P < 0.05$) and decreased firing rate -2.552 ± 1.17 ($P < 0.05$) in 71% of neurons (Fig. 3a–d, Extended Data Fig. 8g, h).

To test whether a magnetic field could remotely modulate neurons *in vivo* to control behaviour, we placed animals close to the electromagnetic coil of an MRI machine (Fig. 3e, f). We reasoned that since hypoglycaemia triggers feeding[17], activation of hypothalamic GK neurons might increase food intake. Magnet treatment of GK–Cre mice with VMH injection of Ad-FLEX-anti-GFP-TRPV1/GFP-ferritin increased blood glucose (Extended Data Fig. 9b–d) and significantly increased food intake after a fast to a similar extent as optogenetic activation of VMH GK–Cre neurons (Fig. 3g). We tested the effect of neural inhibition by magnet treatment of GK–Cre mice with VMH injection of Ad-anti-GFP-TRPV1^{mutant}/GFP-ferritin. Food intake was significantly decreased (Fig. 3h, i). Expression of the activating and inhibitory constructs did not alter baseline blood glucose or food intake (Extended Data Fig. 10) and magnetic field treatment did not affect blood glucose or feeding in wild-type mice after VMH injection of either construct (Extended Data Fig. 9e, f).

Here we show that remote neural modulation of a subpopulation of hypothalamic glucose-sensing neurons changes blood glucose in either direction by regulating pancreatic hormone levels, and that neural activation increases feeding while inhibition decreases it. VMH inhibition to reduce glucose and feeding could be beneficial in metabolic disease. Because activation of the GK neuronal subpopulation mimics the responses to low glucose and inhibiting them blunts this response, we hypothesize that we targeted glucose-inhibited neurons, though further studies will be needed to confirm this, as well as the mechanism by which glucose can inhibit GK-expressing neurons[18,19]. While local particle heating could independently affect mitochondrial UCP2 or other mechanisms, we consider this unlikely because of rapid heat dissipation with distance and the finding that wild-type and mutant TRPV1 had opposite effects[20].

Radio-wave- or magnetic-field-controlled neural modulation provides distinct attributes relative to optogenetics or DREADDs (designer receptors exclusively activated by designer drugs). Unlike optogenetics, the approach does not require a permanent implant so may be suitable when an implant interferes with function or cannot be secured. Further, optogenetics and methods using exogenous nanoparticles[21,22] only target local populations, whereas our genetically encoded system could potentially modulate dispersed populations and/or multiple sites in a circuit simultaneously without requiring multiple implants or nanoparticle injections. The system also enables more rapid responses than DREADDs[23] which activate G protein signalling and the slower kinetics of which[24,25] could affect their utility for neural modulation over short time intervals. Our method could also regulate calcium and/or chloride currents in other, even dispersed, populations such as immune, epithelial and endocrine cells. Pending further efficacy and safety studies and the development of suitable devices, the method could potentially provide a less invasive alternative to deep brain stimulation which requires permanent implants and are sometimes associated with complications[26].

Online Content Methods, along with any additional Extended Data display items and Source Data, are available in the online version of the paper; references unique to these sections appear only in the online paper.

Received 10 August 2015; accepted 28 January 2016.
Published online 23 March 2016.

1. Stanley, S. A., Sauer, J., Kane, R. S., Dordick, J. S. & Friedman, J. M. Remote regulation of glucose homeostasis in mice using genetically encoded nanoparticles. *Nature Med.* **21,** 92–98 (2015).
2. Stanley, S. *et al.* Profiling of glucose-sensing neurons reveals that GHRH neurons are activated by hypoglycemia. *Cell Metab.* **18,** 596–607 (2013).
3. Davies, R., Nakajima, S. & White, N. Enhancement of feeding produced by stimulation of the ventromedial hypothalamus. *J. Comp. Physiol. Psychol.* **86,** 414–419 (1974).
4. Goto, Y., Carpenter, R. G., Berelowitz, M. & Frohman, L. A. Effect of ventromedial hypothalamic lesions on the secretion of somatostatin, insulin, and glucagon by the perfused rat pancreas. *Metabolism* **29,** 986–990 (1980).
5. Shimazu, T., Fukuda, A. & Ban, T. Reciprocal influences of the ventromedial and lateral hypothalamic nuclei on blood glucose level and liver glycogen content. *Nature* **210,** 1178–1179 (1966).
6. Schwartz, M. W. *et al.* Cooperation between brain and islet in glucose homeostasis and diabetes. *Nature* **503,** 59–66 (2013).
7. Kang, L., Routh, V. H., Kuzhikandathil, E. V., Gaspers, L. D. & Levin, B. E. Physiological and molecular characteristics of rat hypothalamic ventromedial nucleus glucosensing neurons. *Diabetes* **53,** 549–559 (2004).
8. Aponte, Y., Atasoy, D. & Sternson, S. M. AGRP neurons are sufficient to orchestrate feeding behavior rapidly and without training. *Nature Neurosci.* **14,** 351–355 (2011).
9. Anthony, T. E. *et al.* Control of stress-induced persistent anxiety by an extra-amygdala septohypothalamic circuit. *Cell* **156,** 522–536 (2014).
10. Nordlie, R. C., Foster, J. D. & Lange, A. J. Regulation of glucose production by the liver. *Annu. Rev. Nutr.* **19,** 379–406 (1999).
11. Bito, H., Deisseroth, K. & Tsien, R. W. CREB phosphorylation and dephosphorylation: a Ca^{2+}- and stimulus duration-dependent switch for hippocampal gene expression. *Cell* **87,** 1203–1214 (1996).
12. Ghosh, A., Ginty, D. D., Bading, H. & Greenberg, M. E. Calcium regulation of gene expression in neuronal cells. *J. Neurobiol.* **25,** 294–303 (1994).
13. Lozano, A. M. & Eltahawy, H. How does DBS work? *Suppl. Clin. Neurophysiol.* **57,** 733–736 (2004).
14. Kühn, F. J., Knop, G. & Luckhoff, A. The transmembrane segment S6 determines cation versus anion selectivity of TRPM2 and TRPM8. *J. Biol. Chem.* **282,** 27598–27609 (2007).
15. Landau, B. R. & Lubs, H. A. Animal responses to 2-deoxy-d-glucose administration. *Proc. Soc. Exp. Biol. Med.* **99,** 124–127 (1958).
16. Kim, T., Moore, D. & Fussenegger, M. Genetically programmed superparamagnetic behavior of mammalian cells. *J. Biotechnol.* **162,** 237–245 (2012).
17. Rowland, N. E., Bellush, L. L. & Carlton, J. Metabolic and neurochemical correlates of glucoprivic feeding. *Brain Res. Bull.* **14,** 617–624 (1985).
18. Evans, M. L. *et al.* Hypothalamic ATP-sensitive K^+ channels play a key role in sensing hypoglycemia and triggering counterregulatory epinephrine and glucagon responses. *Diabetes* **53,** 2542–2551 (2004).
19. Murphy, B. A., Fakira, K. A., Song, Z., Beuve, A. & Routh, V. H. AMP-activated protein kinase and nitric oxide regulate the glucose sensitivity of ventromedial hypothalamic glucose-inhibited neurons. *Am. J. Physiol. Cell Physiol.* **297,** C750–C758 (2009).
20. Horvath, T. L. *et al.* Brain uncoupling protein 2: uncoupled neuronal mitochondria predict thermal synapses in homeostatic centers. *J. Neurosci.* **19,** 10417–10427 (1999).
21. Chen, R., Romero, G., Christiansen, M. G., Mohr, A. & Anikeeva, P. Wireless magnetothermal deep brain stimulation. *Science* **347,** 1477–1480 (2015).
22. Stanley, S. A. *et al.* Radio-wave heating of iron oxide nanoparticles can regulate plasma glucose in mice. *Science* **336,** 604–608 (2012).
23. Armbruster, B. N., Li, X., Pausch, M. H., Herlitze, S. & Roth, B. L. Evolving the lock to fit the key to create a family of G protein-coupled receptors potently activated by an inert ligand. *Proc. Natl Acad. Sci. USA* **104,** 5163–5168 (2007).
24. Alexander, G. M. *et al.* Remote control of neuronal activity in transgenic mice expressing evolved G protein-coupled receptors. *Neuron* **63,** 27–39 (2009).
25. Nawaratne, V. *et al.* New insights into the function of M4 muscarinic acetylcholine receptors gained using a novel allosteric modulator and a DREADD (designer receptor exclusively activated by a designer drug). *Mol. Pharmacol.* **74,** 1119–1131 (2008).
26. Falowski, S. M., Ooi, Y. C. & Bakay, R. A. Long-term evaluation of changes in operative technique and hardware-related complications with deep brain stimulation. *Neuromodulation* **18,** 670–677 (2015).

Acknowledgements We would like to thank A. North, P. Ariel and K. Thomas for help with confocal imaging, D. Acehan and K. Uryu for performing EM studies and S. Korres for assistance with the manuscript. This work was funded by Howard Hughes Medical Institute, the JPB Foundation, the National Institutes of Health (GM095654 and MH105941) and a Rensselaer Fellowship (to J.S.) under an NIH predoctoral training grant (GM067545). Support for this project was provided by a grant from the Robertson Foundation.

Author Contributions J.M.F. conceived the project and supervised the studies. S.A.S. and L.K. designed and performed the experiments. K.L. and S.F.S. provided technical assistance. A.N. assisted with optogenetic studies, J.S. assisted with magnet activation studies and X.Y. assisted with cell culture studies. J.D. provided technical advice for *in vivo* magnet activation studies. J.S.D. provided technical advice. S.A.S., L.K. and J.M.F. wrote the manuscript.

Author Information Reprints and permissions information is available at www.nature.com/reprints. The authors declare no competing financial interests. Readers are welcome to comment on the online version of the paper. Correspondence and requests for materials should be addressed to J.M.F. (friedj@mail.rockefeller.edu).

METHODS

Radiofrequency field and static magnetic field. A 465 kHz sinusoidal signal was provided by a signal generator and applied through an amplifier (both Ultraflex) to a 2-turn solenoid coil with a radius of 2.5 cm to produce an electromagnetic field. The field strengths tested were 31 mT, 27 mT and 23 mT. Samples were placed within the solenoid.

A static magnetic field for imaging experiments was produced using a neodymium-iron-boron permanent magnet (0.25 × 1 inch, axially magnetized, K&J Magnetics). This was able to produce a magnetic flux density of over 5 kilogauss at the magnet surface. Field strengths of 280 mT and 130 mT were generated by increasing the distance from the cells to the magnet surface (2 mm and 5 mm, respectively). A N52 grade neodymium magnet (0.06 × 0.25 inch, axially magnetized, K&J Magnetics) was used for electrophysiological studies. The magnetic field for *in vivo* studies was generated by the superconducting electromagnetic MRI field from a GE 3.0 Tesla Excite HDx MRI Scanner (GE Healthcare). The field strength was measured and regions with strengths of 0.5–1 T or 0.2–0.5 T were used for *in vivo* studies.

Plasmids. Anti-GFP nanobody-TRPV1–2A–GFP ferritin in pEGFPN1 and MSCV-hygro were generated as previously described[1]. Mutation of residue I679K in TRPV1 was performed by site-directed mutagenesis using QuikChange XL Site-Directed Mutagenesis Kit (Agilent). These sequences were cloned into pVQ Ad CMV KNpA for generation of replication deficient adenovirus. To construct Cre- activated recombinant adenovirus vectors, a DNA construct with two pairs of incompatible *lox* sites, *lox*N and *lox*2722, was synthesized and Anti-GFP nanobody-TRPV1–2A–GFP ferritin was cloned between the two pairs in the antisense orientation. The floxed inverted Anti-GFP nanobody-TRPV1–2A–GFP ferritin cassette was then cloned into pVQ Ad CMV KNpA for generation of replication deficient adenovirus. The fidelity of PCR products and cloning was confirmed by DNA sequencing.

Viruses. The recombinant adenoviruses (Ad-CMV-GFP, Ad-CMV-anti-GFP-TRPV1/GFP-ferritin, Ad-FLEX-anti-GFP-TRPV1/GFP-ferritin and Ad-FLEX-anti-GFP-TRPV1^{mutant}/GFP-ferritin were packaged by Viraquest. The final titre was 4×10^{10} plaque-forming units (p.f.u.) per ml. AAV-EF1a-DIO-hChR2(H134R)-eYFP was purchased from UNC Viral Core.

Cell culture and *in vitro* studies. Human embryonic kidney (HEK 293T) cells (ATCC CRL-3216), mycoplasma testing and STR profiling for authentication performed by ATCC) were cultured in DMEM with 10% fetal bovine serum (FBS; Gibco) at 37 °C and 5% CO_2. HEK cells have been reported to be among cell lines that are commonly misidentified. We used HEK 293T cells obtained from and authenticated by ATCC. HEK 293T cells are readily transfected and express transgene products at high levels. Transfected cells were used to examine the sites of TRPV1 and GFP-tagged ferritin expression, to generate stable cells to determine calcium responses to RF and magnetic stimulation and for electrophysiology studies. These studies were also performed in additional cell lines such as N38 (calcium responses), examined *in vivo* (protein expression) or in *ex vivo* slices (electrophysiology). Phoenix ecotropic packaging cells (Stanford University, no authentication or mycoplasma testing) were grown in DMEM with 10% FBS (Gibco) at 37 °C and 5% CO_2. Embryonic mouse hypothalamic N38 cells (Cellutions Biosystems Inc., no authentication, mycoplasma testing performed by Cellultions Biosystems Inc.) were grown in DMEM with 10% FBS at 37 °C and 5% CO_2.

Stable cell lines were produced by retroviral infection of N38 cells using the Phoenix system. Briefly, Phoenix eco cells (2×10^6 cells per 6-cm dish) were transfected with MSCV-hygro anti-GFP-TRPV1/GFP-ferritin or MSCV-hygro anti-GFP-TRPV1^{mutant}/GFP-ferritin. After 24 h, the medium was replaced and the cells placed at 32 °C. Medium was aspirated after a further 24 h and spun to remove cell debris. The Phoenix cell supernatant was added to N38 cells (plated at 1×10^6 cells per 6-cm dish) using a 1:2 dilution in DMEM/10% FBS with polybrene (4 μg ml^{-1}, Sigma-Aldrich). Cells were incubated at 32 °C for a further 24 h before replacing the medium with DMEM/10% FBS. Selection medium was added 48 h after infection. Stably transfected N38 cells were maintained at 32 °C.

For immunocytochemistry, electrophysiology, RF and magnet studies, stably transfected N38 cells or HEK cells were cultured on 12-mm cover glass (Fisher Scientific) coated with fibronectin (10 mg ml^{-1}, Sigma). HEK cells were transfected with appropriate constructs 24 h after plating using lipofectamine 2000 (Invitrogen). Culture medium was replaced 18 h after transfection and holotransferrin (2 mg ml^{-1}, Sigma) was added to the cells. Cells were studied 72–96 h after transfection or subculture.

Effect of RF or magnet on pCREB and c-Fos. 24 h before the study, cells were placed in 1% FBS in optimem medium at 32 °C to ensure minimal activation of TRPV1 and calcium-dependent pathways. On the day of study, cells were incubated in 500 μl of calcium imaging buffer at room temperature (control) or in a RF field (31 mT) at room temperature. For magnet treatment, cells were treated with a static magnetic field (280 mT) for 5 s every 2 min for 1 h at room temperature. After 60 min, the cells were placed on ice, the supernatant removed and cells lysed with RIPA buffer (40 μl for western blot) or lysis buffer (100 μl Agilent Absolutely RNA microprep kit) and frozen at −80 °C until assay or RNA purification. Each study was repeated on three occasions each with four replicates. Control studies with N38 cells alone were performed on two occasions with four replicates.

Calcium imaging. TRPV1 is a non-selective cation channel with relatively high permeability to divalent cations, particularly calcium ($Ca^{2+} > Mg^{2+} > Na^{+} \approx K^{+} \approx Cs^{+}$)[27].

For studies examining the effects of RF (31 mT) or magnet (280 mT) with and without ruthenium red, stably transfected cells were washed three times in PBS then loaded with Fluo-4 3 μM (Invitrogen) in the presence of sulfinpyrazone 500 μM (Sigma) for 45–60 min at room temperature. Cells were washed again in PBS then incubated for 15–30 min in sulfinpyrazone in PBS. Cells were washed and then imaged in calcium imaging buffer. Imaging was performed using a Deltavision personal DV imaging system (Applied Precision) equipped with a custom-made ceramic lens. Images were acquired every 3 s for 3 min. Cells were imaged without treatment (eight occasions), before and during RF treatment (nine occasions), before and during application of a neodymium magnet (for 45 s, three occasions) or before and after treatment with 200 μM 2-APB (two occasions). Imaging was repeated in the presence of ruthenium red (100 μM) (two occasions for each condition). Images were analysed using ImageJ software.

For studies to examine the effects of increasing RF or magnet field strength, to assess the effects of short RF treatment (10 s) on calcium responses and to examine the kinetics of the calcium response, cells were loaded with FluoForte 20 μM (Enzo Life Sciences) in the presence of Pluronic F-127 (0.02% vol/vol) and sulfinpyrazone 500 μM. Cells were washed and then imaged in calcium imaging buffer. Imaging was performed as above with images acquired every second for 1 min. Cells were imaged without treatment (four occasions), before and during RF treatment at 31, 27 and 23 mT (four occasions each), before and during application of a neodymium magnet at 280 or 130mT (magnet 2 mm or 5 mm from the cells, respectively, four occasions each) and before, during and after 10 s treatment with RF (31 mT) (four occasions). Images were analysed using ImageJ software.

Multiphoton chloride imaging. Stably transfected cells were washed with Krebs-HEPES buffer three times then loaded with MQAE (5 mM, Invitrogen) for 60 min at room temperature. The cells were washed with Krebs-HEPES buffer and then incubated in buffer for 15 min before imaging. Imaging was performed using LSM 510 NLO inverted multiphoton and confocal system (Zeiss) using a 40× objective with two photon excitation at 750 nm. Cells were imaged without treatment (four occasions), before and during application of a neodymium magnet (280 mT) for 20 s (on six occasions), before and after treatment with 200 μM 2-APB (two occasions). Imaging was repeated in the presence of ruthenium red (100 μM) (two occasions for each condition). Images were analysed using ImageJ software.

Immunocytochemistry and immunohistochemistry. Immunocytochemistry (ICC) and immunohistochemistry (IHC) were used to detect expression of TRPV1, GFP and Flag-tagged ferritin, to localize c-Fos expression and to quantify apoptosis in cells and tissue. Cells were washed twice in PBS and then fixed for 15 min in 2% paraformaldehyde (Electron Microscopy Services). Tissue was fixed in 10% formalin (Sigma) at 4 °C overnight and 40-μm sections cut on a vibrating microtome. Fixed cells or tissue sections were washed then incubated for 1 h in blocking buffer (3% BSA (Sigma) and 2% goat serum (Sigma) in PBS with 0.1% Triton-X (Sigma)). Cells and tissues were then incubated in primary antibody (rabbit anti-TRPV1 1:500 (AB9554[1], Chemicon), mouse anti-Flag 1:1,000 (Flag-tag mouse monoclonal antibody #F3165, Sigma[28]), chicken anti-GFP 1:1,000 (ab13970[1], Abcam), rabbit anti-activated-caspase-3 1:250 (G7481, Promega[1]) or rabbit anti-c-Fos 1:5,000 (PC38, Calbiochem[2])) diluted in blocking buffer overnight at 4 °C. Cells or tissue were washed three times in PBS/0.1% Triton-X before incubation in secondary antibody (goat anti-rabbit 594 (A1012) or goat anti-rabbit 488 (A11008), goat anti-chicken 488 (A11039), goat anti-mouse 350 (A11045), all 1:1,000) diluted in blocking buffer for 2 h. To stain for cell membrane, Alexa 594 conjugated to wheat germ agglutinin (Invitrogen, 5 μg ml^{-1}) was included in the blocking buffer with secondary antibodies. The cells or tissue were washed a further three times in PBS/0.1% Triton-X before mounting using Fluoromount (Southern Biotech).

Images were acquired using confocal microscopy (LSM 510 laser scanning confocal microscope; Carl Zeiss MicroImaging, Inc.). Confocal fluorescence images were acquired on a scanning laser microscope using a 20×/0.70 NA objective or 100×/1.4 NA objective. To quantify GFP-positive and activated-caspase-3-positive cells, a 1,280 μm section of the brain with the injection site taken as the centre was imaged by taking tiled, serial stack images covering a depth of 40 μm every 320 μm. Quantification of GFP and activated-caspase-3 immunostaining was performed by an investigator blinded to the treatment group using Imaris

3D quantification software. The image analysis software calculated the number of GFP- or activated-caspase-3-positive cells per volume by thresholding immunoreactivity above background levels. Confocal images to examine co-localization of TRPV1, GFP and Flag-tagged ferritin were acquired with a 40× objective.

Immuno-electron microscopy and electron microscopy. Mouse brains were perfused by 4% PFA and sectioned at 50 μm by vibratome (Leica VT 100S). The sections were blocked by 4% BSA and 0.15% saponin in 20 mM Tris buffer (pH 7.4) for 2 h at room temperature, then incubated with anti-GFP (1:1,000) (#1020, Aves Lab Inc.[29]) overnight at 4 °C, followed by biotinylated anti-chicken incubation (1:1,000, Vector Laboratories, Inc.), with Nanogold streptavidin (1:100, Nanoprobes), and treated with GoldEhance EM (#2114 Nanoprobes). Negative control was done with the same procedure, except for omitting the primary antibody incubation. The tissue sections underwent fixation with 2% glutaraldehyde in sodium cacodylate buffer, light osmication (0.5% osmium tetroxide) for 15 min and en bloc staining with 1% uranium acetate for 30 min. Subsequently tissues were dehydrated through an ethanol series followed by incubation with Eponate12 (Ted Pella Inc.) The samples were embedded in the resin and polymerized at 60 °C for 48 h. Ultrathin (70 nm) sections were cut and examined under a JEOL JEM 100CX transmission electron microscope in the electron microscopy centre in The Rockefeller University.

For double immuno-electron microscopy studies, HEK cells with stable expression of TRPV1 without fixation were subjected to high-pressure freezing (Leica EMPAC2) and freeze substitution in 0.2% uranyl acetate in 95% acetone and 5% water. Subsequently they were embedded in Lowicryl HM20 at −40 °C and cut into ultrathin sections. They were incubated with 4% BSA and 0.15% saponin, 0.15% cold fish skin gelatin in 20 mM TBS (pH 7.4) for 2 h at room temperature, a mixture of anti-GFP raised in chicken (1:300) (Aves Lab Inc.) and anti-TRPV1 raised in rabbit (1:300) (EMD Millipore Corp) overnight at 4 °C. Antigen–antibody complexes were recognized by biotinylated anti-chicken antibody and streptavidin tagged with 5 nm colloidal gold (1:20, Nanoprobes), or anti-rabbit tagged with 12 nm colloidal gold (Jackson Immuno Research Lab Inc.) for 2 h at room temperature.

Electron microscopy was used to demonstrate ferritin in transfected HEK cells. Cells were fixed in 2% paraformaldehyde/2.5% glutaraldehyde/0.1 M cacodylate buffer, pH 7.4, for 15 min before pelleting and further fixation for 1 h. Cells were then treated with 1% osmium tetroxide (1 h, on ice) and 0.5% uranyl acetate (1 h) before dehydration with graded ethanol and treatment with propylene oxide (2 × 15 min). The cells were infiltrated with 50% EPON epoxy resin (Miller-Stephenson) and 50% propylene oxide overnight then 100% EPON (2 × 2 h) before curing at 60 °C for 2 days. Blocks were cut with a diamond knife on a Leica UltracutE and ultrathin (~70 nm) sections were collected on uncoated 200-mesh grids and stained with uranium and lead. Grids were viewed with a Tecnai SpiritBT Transmission Electron Microscope (FEI) at 80 kV and pictures were taken with Gatan 895 ULTRASCAN Digital Camera in the electron microscopy centre in The Rockefeller University.

Electrophysiology. *Cell culture.* Whole-cell voltage clamp recordings were made at room temperature at −60 mV from cultured HEK cells and N38 cells expressing anti-GFP–TRPV1/GFP–ferritin or anti-GFP–TRPV1^{mutant}/GFP–ferritin construct. Neurons expressing GFP were visualized using epifluorescence on an upright Zeiss Axioskop 2FS Plus microscope equipped with a Hamamatsu CCD camera. External solution contained (in mM): 140 NaCl, 2.8 KCl, 2 $CaCl_2$, 1 $MgCl_2$, 1 HEPES, 10 glucose, pH 7.4. Patch pipettes pulled from borosilicate glass (World Precision Instruments) had tip resistances of 5–10 MΩ and were filled with K-gluconate internal containing (in mM): 135 potassium gluconate, 4 KCl, 0.05 EGTA, 10 HEPES, 4 MgATP, 10 Na-phosphocreatine, pH adjusted to 7.3 with KOH, 290 OSM unless otherwise stated, in which case a CsCl internal solution was used containing (in mM):125 CsCl, 10 HEPES, 10 EGTA, 4 MgATP, 0.5 $CaCl_2$, 2-APB (200 μM) was prepared from a 10 mM DMSO stock and was perfused though the bath when stated. I–V relationships were obtained by measuring current responses to increasing 5-mV steps in the presence of 200 μM 2-APB. Cells were held at −60 mV. Magnetic activation was applied by bringing a permanent magnet within 500 μm of the recorded cell for 5 s with a micromanipulator. Recordings were acquired with an Axopatch 200B amplifier, filtered to 2 kHz and digitized at 10 kHz (pClamp10 software, Molecular Devices). Data were analysed using IGOR Pro (Wavemetrics) and NeuroMatic (http://www.neuromatic.thinkrandom.com/). Series resistance was monitored and not compensated for. If there was more than a 20% change in series resistance the recording was excluded.

Slice electrophysiology. Glucokinase–Cre Rosa–tdTomato, injected with Ad-anti-GFP-TRPV1/GFP-ferritin or Ad-anti-GFP-TRPV1^{mutant}/GFP-ferritin in the VMH were deeply anaesthetized with isoflurane before decapitation and removal of the entire brain to be immediately submerged in ice-cold 'slicing' solution containing (in mM): 85 NaCl, 2.5 KCl, 0.5 $CaCl_2$, 4 $MgCl_2$, 25 $NaHCO_3$, 1.25 NaH_2PO_4, 64 sucrose, 25 glucose and 0.02 D-2-amino-5-phosphonopentanoic acid (D-AP5, Tocris Bioscience). This was bubbled with 95% O_2 and 5% CO_2, pH 7.4. Coronal hypothalamic slices (200 μm) were made with a moving blade microtome (VT1000S, Leica). The slices were kept at 32 °C for 40 min in recording solution containing (in mM) 125 NaCl, 2.5 KCl, 1.25 NaH_2PO_4, 26 $NaHCO_3$, 10 glucose, 2 $CaCl_2$ and 1 $MgCl_2$, pH 7.4 when bubbled with 95% O_2 and 5% CO_2. Whole-cell current-clamp patch-clamp recordings were made at room temperature from neurons in the VMH expressing both tdTomato indicating GK–Cre expression and GFP indicating expression of the anti-GFP–TRPV1/GFP–ferritin or anti-GFP–TRPV1^{mutant}/GFP–ferritin construct. Neurons were visualized and recorded from as described above. In order to observe neuronal activation, neurons were hyperpolarized to below threshold.

Baseline characteristic for hypothalamic neurons are as follows. Mean series resistance for neurons expressing the construct was 18.4 ± 1.1 MΩ (n = 37) and did not differ significantly from hypothalamic neurons that did not express the construct (18.0 ± 1, n = 7). The mean capacitance was 5.1 ± 0.55 pF and did not differ significantly from neurons not expressing the channel (6.7 ± 0.8) The mean resting membrane potential in naive hypothalamic neurons was −48.21 ± 4.7 mV (n = 15) and in cells expressing the construct before manipulation was −52 ± 1.9 mV (n = 37), P > 0.5. Input resistances did not significantly differ in hypothalamic neurons; control neuron (without construct expression) = 703 ± 128 MΩ (n = 13), wild-type channel neuron = 555 ± 110 MΩ (n = 7), mutant neuron = 866 ± 220 MΩ (n = 14).

Animals and *in vivo* studies. Male and female C57Bl6 mice (8–9-weeks-old, Jackson Laboratories), *Nestin cre* (8–9-weeks-old, Jackson Labs), *Rosa lox-stop-lox tdTomato* (8–10-weeks-old, Jackson Labs) and *GK-cre* (8–16-weeks-old) mice were used and housed under controlled light conditions (12 h light/12 h dark) and temperature (22 °C), single-caged, and fed *ad libitum* on standard mouse chow. Animal care and experimental procedures were performed with the approval of the Animal Care and Use Committee of Rockefeller University (protocols 12561 and 14712) under established guidelines. In all cases, mice were randomized according to body weight. The investigator was not blinded to the treatment group. The sample size required was estimated to be n = 8–10 per group on the basis of previous studies examining the effects of RF treatment on gene expression and protein release. No statistical methods were used to predetermine sample size.

All surgeries were performed under aseptic conditions. Mice were anaesthetized using 1.5% isoflurane and the top of the head was shaved then cleaned with 70% ethanol. An incision was made in the midline and small craniotomies were made using a dental drill.

Study 1. Wild-type mice underwent stereotacic injection into the striatum (coordinates: +1 mm AP, +2.3 mm ML, −3.3 mm DV) with Ad-CMV-GFP or Ad-CMV-anti-GFP-TRPV1/GFP-ferritin (4×10^8 p.f.u. per injection) over 10 min. The needle remained in position for a further 5 min before being withdrawn. Mice also received a lateral ventricle injection of iron dextran (4 μl, coordinates: −0.4 mm AP, +1.2 mm ML, −2.0 mm DV). After 1 week or 4 weeks, mice injected with Ad-CMV-anti-GFP-TRPV1/GFP-ferritin were randomized to RF or no RF treatment (n = 4 per time point and per treatment group). All mice treated with Ad-CMV-GFP were treated with RF (n = 4 per time point). Mice were anaesthetized with tribromoethanol (200 mg kg^{-1}) and after 15 min mice were treated with RF (Ad-GFP and Ad-CMV-anti-GFP-TRPV1/GFP-ferritin, RF-treated group) for 30 min by placing in the RF solenoid. Ad-CMV-anti-GFP-TRPV1/GFP-ferritin, untreated group were anaesthetized and 15 min after the induction of anaesthesia were placed in the RF solenoid without power for 30 min. One hour after the being placed in the solenoid, mice were perfused, brains removed and tissue processed for GFP and activated-caspase-3 immunostaining as described above.

Unilateral striatal injections were used to test our construct primarily because we thought that either basal activity in the absence of RF or significant toxicity and apoptosis would result in motor changes that are readily detectable. In addition, striatum does not express TRPV1 and we wanted to ensure any effect was the result of expressing our construct rather than a result of an effect of endogenous TRPV1. Finally, for RF treatment the mice needed to be anaesthetized and in pilot studies we found that anaesthetics often led to high levels of c-Fos activation in many central nervous system regions but not in the striatum. Thus, to minimize the possibility that the anaesthetic was contributing to either toxicity or non-specific staining, we used striatal injections in addition to assessing the VMH.

Study 2. Nestin–Cre or wild-type mice received striatal injections of Ad-FLEX-anti-GFP-TRPV1/GFP-ferritin (4×10^8 p.f.u. per injection) and ICV iron dextran as described above. After 1 week, mice were anaesthetized, treated with RF for 30 min and perfused after 1 h as described above. Tissue was processed for GFP and c-Fos immunostaining as described above.

Study 3. Glucokinase–Cre or wild-type mice were anaesthetized with isofluorane and underwent stereotactic injection of iron dextran into the lateral ventricle

(as above) and unilateral injection of Ad-FLEX-anti-GFP-TRPV1/GFP-ferritin (4×10^8 p.f.u. per injection) into the VMH (coordinates: −0.9 mm AP, +0.32 mm ML and −5.48 mm DV). We performed unilateral injections of Cre-dependent adenovirus into the dorsomedial VMH of glucokinase–Cre mice. Construct expression was seen in this subdivision and in additional subdivisions of the VMH on the injected side. Virus expression is Cre-dependent as we did not see GFP expression in wild-type mice. After 1 week, half the mice in each group were studied using RF stimulation (31 mT) and half remained untreated. One week later, the previously treated mice were assessed without RF treatment and the previously untreated mice were treated with RF. Tail vein samples for blood glucose were taken at −5, 0, 5, 10, 20, 30, 45, 60 and 90 min after the onset of RF treatment. After an additional week, mice were treated as described above but at 60 min after the onset of RF treatment, mice were killed and blood taken by cardiac puncture for hormone assessment and hepatic tissue was harvested and snap-frozen in liquid nitrogen for later assessment of gluconeogenic enzyme expression. Brains were fixed, sectioned and stained with GFP to check injection placement. Mice with injection sites outside the VMH were excluded from the analysis.

Study 4. GK–Cre mice were anaesthetized and injected with AAV-EF1a-DIO-hChR2(H134R)-EYFP (1 μl) into the VMH using the coordinates above. An optic fibre was then placed 200 nm above the injection site and fixed with adhesive cement followed by dental cement then the scalp was sealed back using tissue adhesive. After 4 weeks, half the mice were treated with 473 nm laser stimulation (5 Hz, 15 ms pulse width) for 30 min and half were attached to the optical cable but without light stimulation. One week later, the previously treated mice were assessed without light treatment and the previously untreated mice were treated with light. Tail vein samples for blood glucose were taken at −5, 0, 5, 10, 20, 30, 45, 60 and 90 min after the onset of light treatment. Brains were fixed, sectioned and stained with GFP to check injection placement. Mice with injection sites outside the VMH were excluded from the analysis.

Study 5. GK–Cre or wild-type mice were anaesthetized with isofluorane and underwent stereotactic injection of iron dextran into the lateral ventricle (as above) and Ad-FLEX-anti-GFP-TRPV1^{mutant}/GFP-ferritin (4×10^8 p.f.u. per injection) into the VMH. After one week, half the mice in each group were studied using RF stimulation (31 mT) and half remained untreated. One week later, the previously treated mice were assessed without RF treatment and the previously untreated mice were treated with RF. Tail vein samples for blood glucose were taken at −5, 0, 5, 10, 20, 30, 45, 60 and 90 min after the onset of RF treatment. After a further 3 days, mice were anaesthetized and at time 0 were treated with 2-deoxyglucose (400 mg kg^{-1}, intraperitoneal) then treated with RF for 45 min. Tail vein samples for blood glucose were taken at −5, 0, 5, 10, 20, 30, 45, 60 and 90 min after the onset of RF treatment. One week later, mice were anaesthetized and RF treated (31 mT) and at 60 min after the onset of RF treatment, they were killed and blood taken by cardiac puncture for hormone assessment and hepatic tissue was harvested and snap frozen in liquid nitrogen for later assessment of gluconeogenic enzyme expression. Brains were fixed, sectioned and stained with GFP to check injection placement. Mice with injection sites outside the VMH were excluded from the analysis.

Study 6. GK–Cre or wild-type mice were anaesthetized with isofluorane and underwent stereotactic injection of iron dextran into the lateral ventricle and Ad-FLEX-anti-GFP-TRPV1/GFP-ferritin (4×10^8 p.f.u. per injection) into the VMH (as above). After one week, mice were placed in a plastic chamber in a low-strength magnetic field (<0.005 T) for a 15 min acclimation period, then half the mice were moved to a high-strength magnetic field (>0.5 T) for 30 min and half remained in the low-strength field. After 30 min, all mice were placed in a low-strength field for a further 30 min. Tail vein samples for blood glucose were taken at −5, 0, 15, 30, 45 and 60 min after the acclimation period. One week later, groups were crossed so the mice previously treated with high-strength magnetic field were treated with low-strength field and mice previously treated with low-strength field were treated with high-strength magnetic field. At the end of the study, mice were sacrificed and perfused. Brains were fixed, sectioned and stained with GFP to check injection placement. Mice with injection sites outside the VMH were excluded from the analysis.

Study 7. GK–Cre or wild-type mice were injected and recovered as in study 6. After one week, the effect of magnetic field stimulation on food intake was examined. After a 4-h fast, mice were acclimated to their chamber for 20 min then food intake was assessed after 20 min at low-strength magnetic field. Food intake was then measured for 20 min with half the mice in high-strength magnetic field (0.5–1 T) and half at low-strength magnetic field. Food intake was measure for a final 20 min period at low-strength magnetic field. One week later, the groups were crossed so mice previously treated with high-strength magnetic field were treated with low-strength field and mice previously treated with low-strength field were treated with high-strength magnetic field. At the end of the study, mice were sacrificed and perfused. Brains were fixed, sectioned and stained with GFP to check injection placement. Mice with injection sites outside the VMH were excluded from the analysis.

Study 8. GK–Cre mice underwent stereotactic injection as described in study 3. After one week, mice were anaesthetized and 15 min after the induction of anaesthesia were placed in the RF solenoid without power for 30 min (no RF treatment). After 3 days, the mice were divided into two equal groups, one group was treated with a field strength of 27 mT for 30 min and the other group with a field strength of 23 mT for 30 min. After a further 4 days, the treatment groups were reversed. A week later, the first group of mice were treated with RF (31 mT) for 20 min and the second group of mice with RF (31 mT) for 10 min. After a further 3 days, the treatment groups were reversed. Tail vein samples for blood glucose were taken at −5, 0, 5, 10, 20, 30, 45, 60 and 90 min after the onset of RF treatment for all studies. After an additional week, half the mice were treated with RF (31 mT) for 30 min and half the mice remained untreated. At 60 min after the onset of RF treatment, mice were sacrificed and brains were fixed, sectioned and stained for GFP and activated-caspase-3 to assess apoptosis in the VMH.

Study 9. GK–Cre mice underwent stereotactic injection as described in study 3. After 2 weeks, the effects of lower magnetic strength (0.2–0.5 mT) on food intake were assessed. After a 4-h fast, mice were acclimated to their chamber for 20 min and then food intake was assessed after 20 min at low-strength magnetic field followed by food intake measurement after 20 min treatment with a 0.2–0.5 T magnetic field. Food intake was measure for a final 20 min period at low-strength magnetic field. At the end of the study, mice were sacrificed and perfused. Brains were fixed, sectioned and stained with GFP to check injection placement.

Study 10. GK–Cre mice underwent stereotactic injection as described in study 5 but with bilateral injection of Ad-FLEX-anti-GFP-TRPV1^{mutant}/GFP-ferritin into the VMH. After a week, food intake was assessed in response to low-strength magnetic field treatment. After a 4-h fast, mice were acclimated to their chamber for 20 min and then food intake was measured for three periods of 20 min at low field strength. One week later, the study was repeated with a 20 min acclimation period then food intake was measured for mice were treated with high strength magnetic field (0.5–1 T) for 20 min. Food intake was measured for a further two 20-min periods at low magnetic field strength. At the end of the study, mice were sacrificed and perfused. Brains were fixed, sectioned and stained with GFP to check injection placement.

Study 11. GK–Cre/Rosa–tdTomato mice underwent stereotactic surgery as described in study 3. After one week, three mice were anaesthetized and 15 min after the induction of anaesthesia were treated with RF (31 mT) for 30 min. At 60 min after the onset of RF treatment, mice were sacrificed. Brains from three mice were fixed, sectioned and stained for GFP and c-Fos. The fourth mouse was perfused without RF treatment and the brain was used for immune-electron microscopy.

Study 12. GK–Cre ($n = 4$) underwent stereotactic surgery as described in study 3. After one week, the mice were anaesthetized and perfused. Brains were fixed, sectioned and stained for GFP. Tiled *z*-stack images were taken using confocal microscopy (20× objective) and images analysed using Imaris 3D quantification software. The image analysis software calculated the number of GFP-positive cells per volume by thresholding immunoreactivity above background levels. Using this method the average number of GFP-positive cells was 2,436 ± 841 cells per brain.

Assays. Blood glucose was determined using a Breeze 2 glucometer (Bayer). Blood was spun for 10 min and plasma was collected. Plasma levels of insulin (Mercodia) and glucagon (Mercodia) were determined by ELISA.

Western blot. Protein was isolated by lysis in RIPA buffer and centrifugation at 16,000 r.p.m., 4 °C for 5 min before addition of 4× Laemelli buffer. Samples were denatured for 5 min at 95 °C and frozen at −20 °C before assay. Samples (15 μl) were run on a 4–15% gel then transferred to PVDF membrane. Membranes were blocked (3% dried milk in TBST buffer) for 1 h at room temperature then incubated in primary antibody (pCREB (Ser133) (87G3) rabbit monoclonal antibody (1:1,000) or β-actin rabbit antibody (1:1,000), Cell Signaling) in TBST overnight at 4 °C. Membranes were washed three times in TBST then incubated in secondary antibody (goat anti-rabbit IgG-HRP, 1:5,000, Santa Cruz) in TBST for 2 h at room temperature. The membrane was washed a further five times then developed in substrate for 5 min (Supersignal West Femto maximum sensitivity substrate, Life Technologies) and imaged (C-DiGit blot scanner, Licor). The pCREB density signal was corrected for any variation in protein loading by dividing by the density signal for the housekeeping gene, actin.

Real-time PCR. Total RNA was isolated by homogenizing tissue in TRIzol reagent (Invitrogen) or cells in buffer RLT and purifying the RNA using Absolutely RNA microprep kit (Agilent). Complimentary DNA was synthesized using QIAGEN omniscript RT kit. Real-time PCR was performed using the TaqMan system (Applied Biosystems) according to the manufacturer's protocol.

Statistics. Data over 2 s.d. outside the mean were excluded from further analysis as determined before the studies. All data were tested for Gaussian distribution and variance. Data with normal distribution and similar variance were analysed for statistical significance using two-tailed, unpaired Student's *t*-tests unless otherwise indicated. Data with normal variation and unequal variance were analysed by two-tailed Welch's *t*-tests. Paired data were analysed by paired *t*-tests. Data with more than two groups were analysed by one-way ANOVA with post-hoc Tukey's analysis for parametric data. Data which were not normally distributed were analysed by two-tailed Mann–Whitney *U*-tests or Kruskal–Wallis tests with post-hoc Dunn's correction. *P* values are as indicated. Time course data were analysed by two-way ANOVA with Sidak's multiple comparisons or repeated measures two-way ANOVA with Sidak's multiple comparisons for paired data. Data are shown as mean ± s.e.m. unless otherwise stated.

27. Caterina, M. J. *et al.* The capsaicin receptor: a heat-activated ion channel in the pain pathway. *Nature* **389,** 816–824 (1997).
28. Wu, S. Y. & Chiang, C. M. Expression and purification of epitope-tagged multisubunit protein complexes from mammalian cells. *Curr. Protoc. Mol. Biol.* Chapter 16, Unit 16.13 (2002).
29. Nakaya, N., Sultana, A., Lee, H. S. & Tomarev, S. I. Olfactomedin 1 interacts with the Nogo A receptor complex to regulate axon growth. *J. Biol. Chem.* **287,** 37171–37184 (2012).

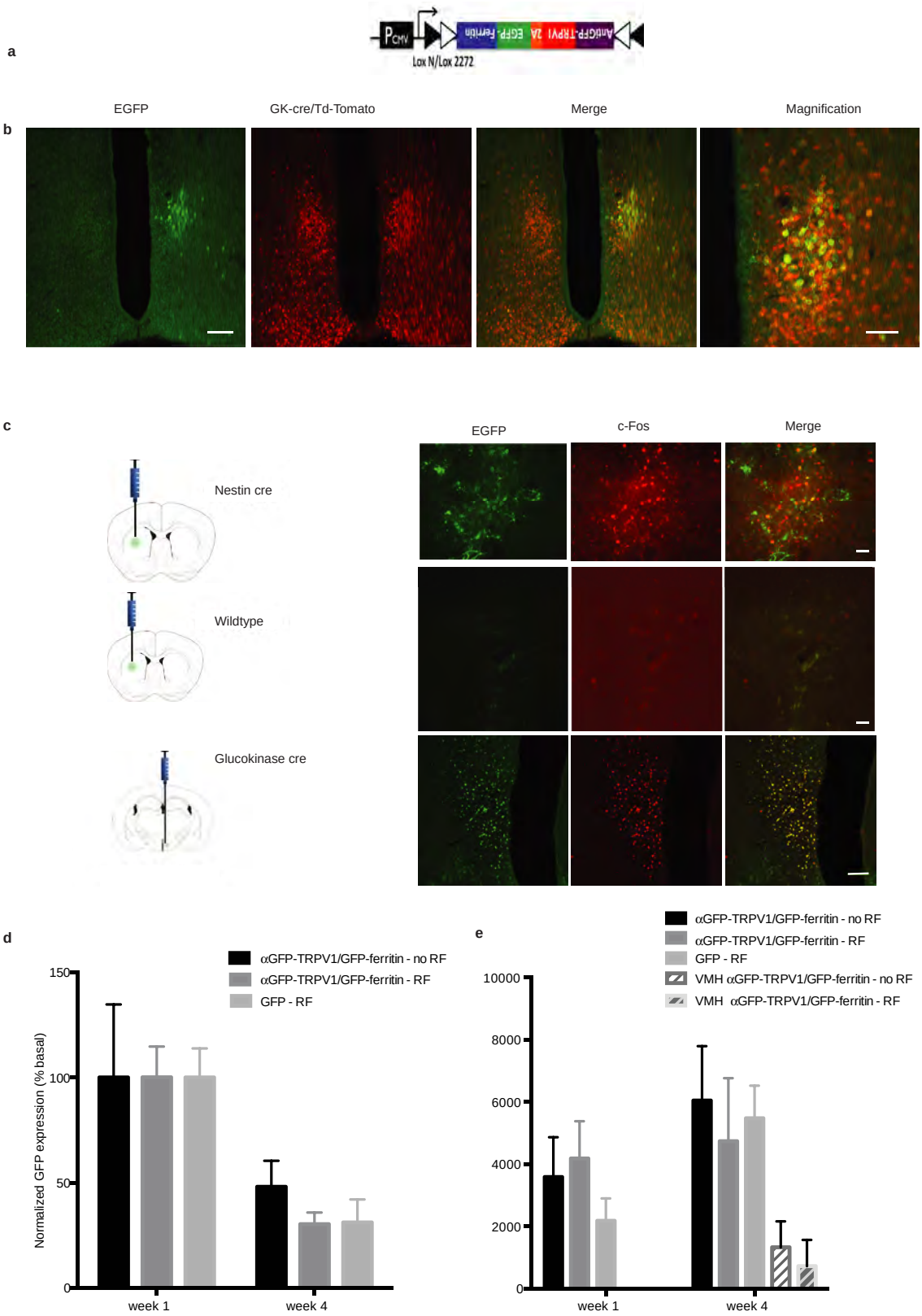

Extended Data Figure 1 | Remote neural activation using RF *in vivo*. **a**, Construct design for Ad-FLEX-anti-GFP-TRPV1/GFP-ferritin. CMV, cytomegalovirus promoter. *lox*N and *lox*2272 are orthogonal recombination sites. **b**, Immunostaining for eGFP in GK–Cre/tdTomato mice demonstrates expression of the GFP in glucokinase neurons after VMH injection of Ad-FLEX-anti-GFP-TRPV1/GFP-ferritin. Scale bars, 100 μm; 50 μm in magnification panel. **c**, Co-localization between eGFP and c-Fos after RF treatment of Nestin–Cre (upper panels) or wild-type (middle panels) mice injected with Ad-FLEX-anti-GFP-TRPV1/GFP-ferritin into the striatum (Scale bar, 80 μm) and of GK–Cre mice injected with Ad-FLEX-anti-GFP-TRPV1/GFP-ferritin into the VMH (lower panels). Scale bar, 100 μm. Quantification of GFP (**d**) and activated-caspase-3 (**e**) immunostaining in mice following injection of Ad-anti-GFP-TRPV1/GFP-ferritin or Ad-GFP (1 μl) into the striatum of wild-type (WT) mice or injection of Ad-FLEX-anti-GFP-TRPV1/GFP-ferritin into the VMH of GK–Cre mice. In all cases, columns represent mean and error bars indicate s.e.m. Data were analysed by Kruskal–Wallis test with post-hoc Dunn's correction. $n = 4$ mice per group.

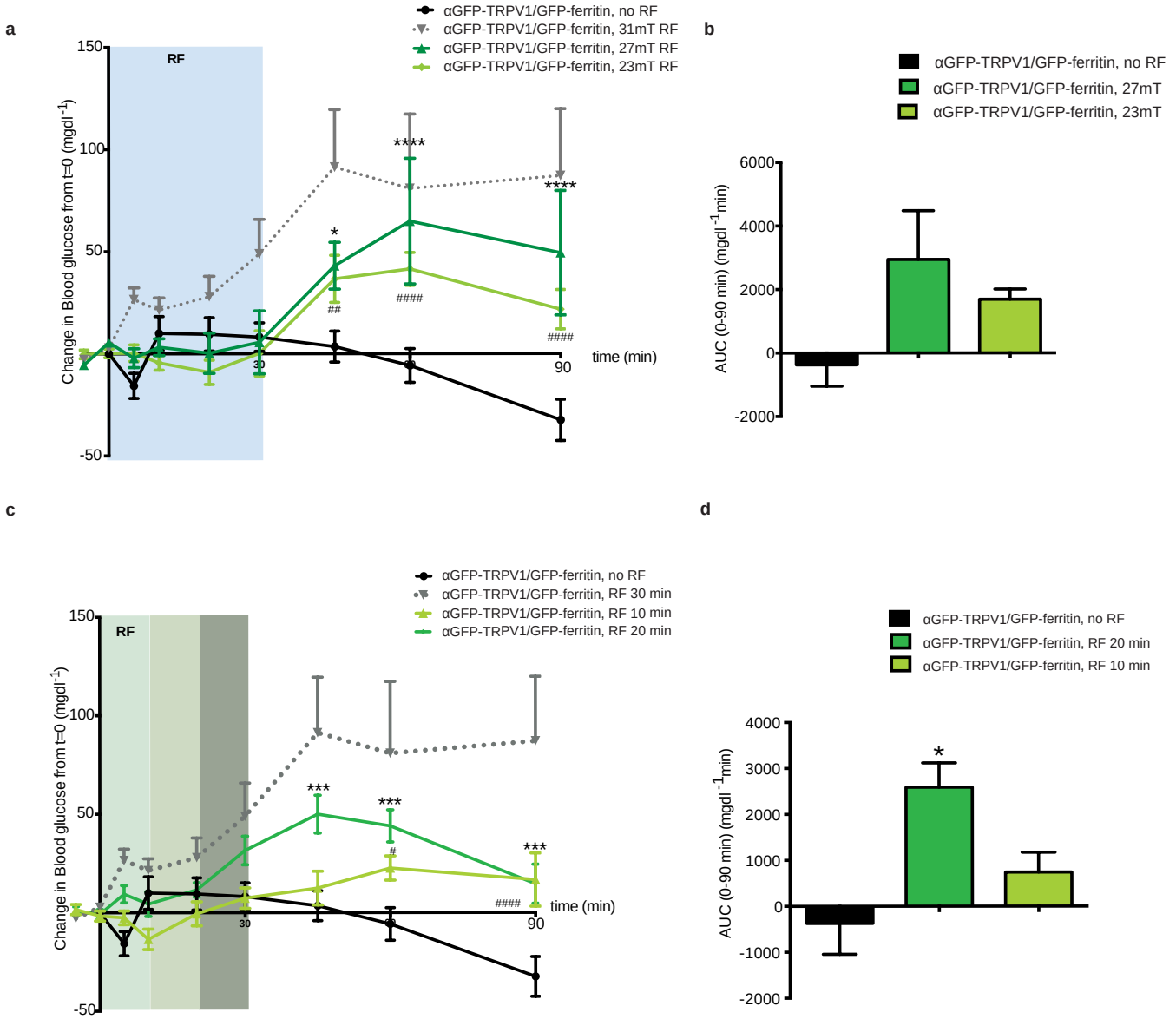

Extended Data Figure 2 | Effects of RF field strength and treatment duration *in vivo*. **a**, Effect of increasing RF field strength on the change in blood glucose and **b**, the cumulative change in blood glucose in GK–Cre mice with VMH injection of Ad-FLEX-anti-GFP-TRPV1/GFP-ferritin. Data are shown as mean and error bars indicate s.e.m. Data were analysed by two-way ANOVA with Sidak's multiple comparisons. * or # indicates $P < 0.05$, ** or ## indicates $P < 0.01$, *** or ### indicates $P < 0.001$, **** or #### indicates $P < 0.0001$ between treated and untreated groups. **c**, Effect of increasing RF treatment duration on the change in blood glucose and **d**, the cumulative change in blood glucose in GK–Cre mice with VMH injection of Ad-FLEX-anti-GFP-TRPV1/GFP-ferritin. Data are shown as mean and error bars indicate s.e.m. Data were analysed by two-way ANOVA with Sidak's multiple comparisons. * or # indicates $P < 0.05$, ** or ## indicates $P < 0.01$, *** or ### indicates $P < 0.001$, **** or #### indicates $P < 0.0001$ between treated and untreated groups.

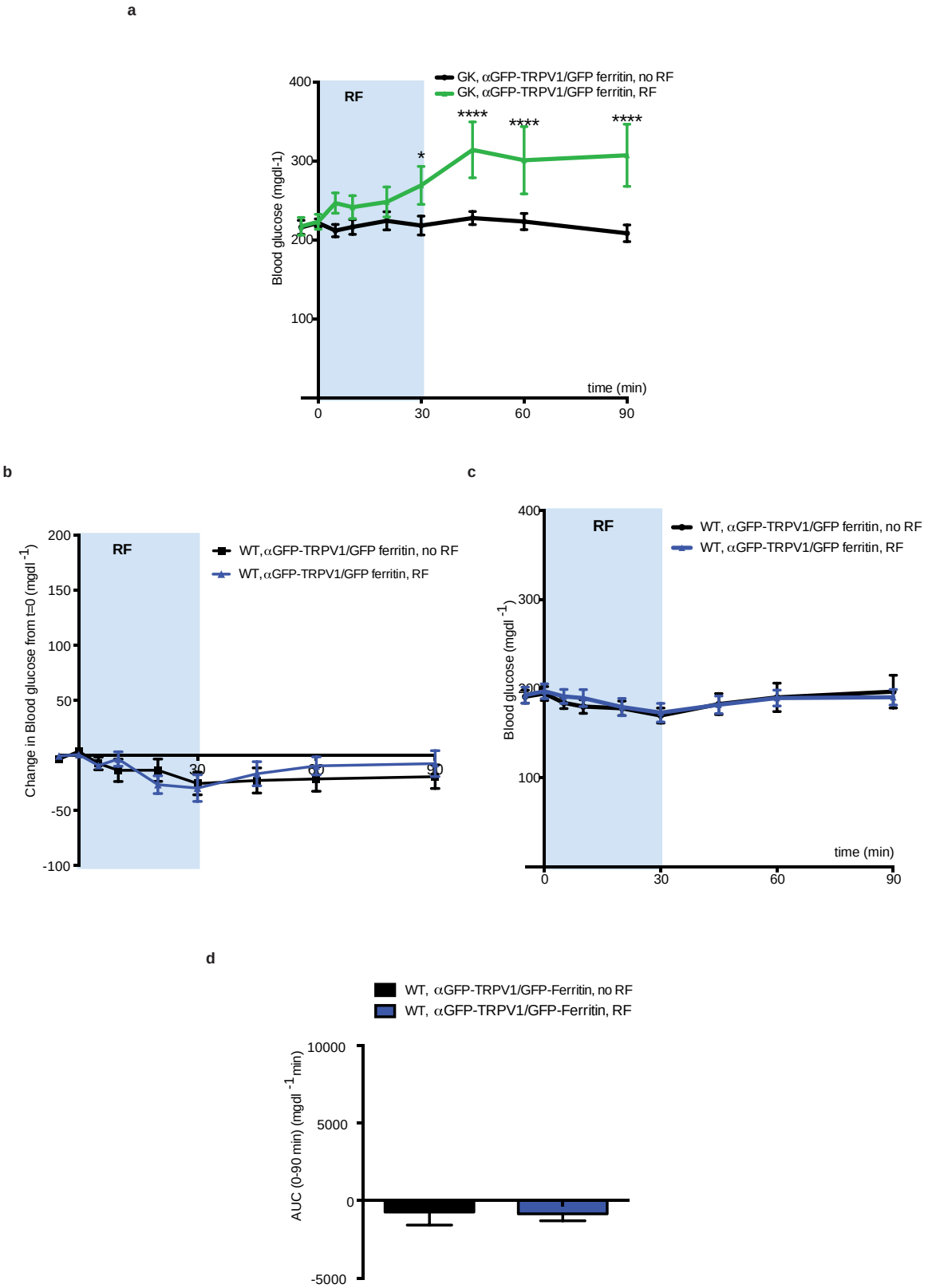

Extended Data Figure 3 | See next page for caption.

Extended Data Figure 3 | Neural activation in GK–Cre and wild-type mice *in vivo*. **a**, RF treatment of GK–Cre mice expressing anti-GFP-TRPV1/GFP-ferritin in the VMH significantly increases blood glucose compared to no RF treatment ($n = 13$). Data points indicate mean and error bars indicate s.e.m. Data were analysed by two-way ANOVA with Sidak's multiple comparisons. $^{*}P < 0.05$, $^{**}P < 0.01$, $^{***}P < 0.001$, $^{****}P < 0.0001$ between treated and untreated groups. **b**, Effects of RF treatment of wild-type mice injected with anti-GFP–TRPV1/GFP–ferritin in the VMH on change in blood glucose with time ($n = 10$). Data points indicate mean and error bars indicate s.e.m. Data were analysed by two-way ANOVA with Sidak's multiple comparisons. **c**, Effects of RF treatment of wild-type mice injected with anti-GFP–TRPV1/GFP–ferritin in the VMH on blood glucose with time ($n = 10$). Data points indicate mean and error bars indicate s.e.m. Data were analysed by two-way ANOVA with Sidak's multiple comparisons. **d**, Effect of RF treatment on cumulative change in blood glucose over the course of the study in wild-type mice with VMH injection of anti-GFP–TRPV1/GFP–ferritin ($n = 10$). Columns represent mean and error bars indicate s.e.m. Data were analysed by two-tailed, paired Student's *t*-test.

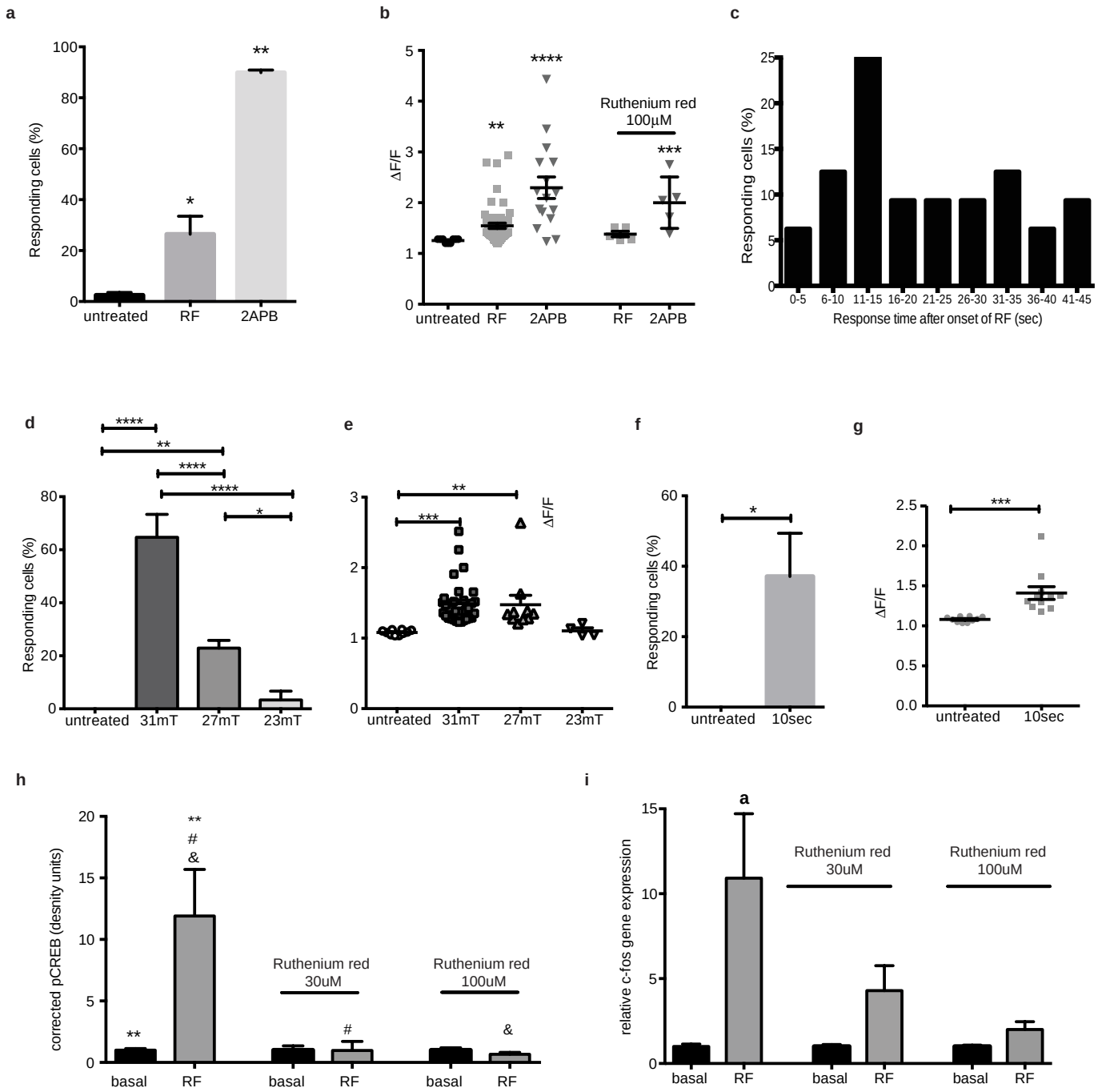

Extended Data Figure 4 | Remote neural activation of N38 cells expressing anti-GFP–TRPV1/GFP–ferritin *in vitro*. **a**, Calcium imaging of RF-treated N38 cells expressing anti-GFP–TRPV1/GFP–ferritin showing the percentage of cells responding (>20% increase in fluorescence) to no treatment, RF or 2-APB ($n = 8$, 9 or 2 occasions, respectively), **b**, the increase in fluorescent signal with RF or 2-APB treatment that is inhibited by Ruthenium red and **c**, the response time (to reach 20% increase in fluorescence) to RF treatment ($n = 38$ cells). Data are represented as mean and error bars indicate s.e.m. Data were analysed by Kruskal–Wallis test with Dunn's multiple comparison test. $^{*}P < 0.05$ vs. untreated, $^{**}P < 0.01$ vs. untreated, $^{***}P < 0.001$ vs. untreated and $^{****}P < 0.0001$ vs. untreated. **d**, Calcium imaging in stably transfected N38 cells expressing anti-GFP–TRPV1/GFP–ferritin demonstrates a field-strength-dependent increase in the percentage of responding cells (>20% increase in fluorescence) and **e**, the fluorescent signal in compared to untreated cells; $n = 10$, 33, 10 and 4 cells, respectively. Data points indicate mean and error bars indicate s.e.m. Data were analysed by two-way ANOVA with Sidak's multiple comparisons. $^{*}P < 0.05$, $^{**}P < 0.01$, $^{***}P < 0.001$ $^{****}P < 0.0001$ between treated and untreated groups. **f**, RF treatment of stably transfected N38 cells expressing anti-GFP–TRPV1/GFP–ferritin for 10 s significantly increases the percentage of responding cells and **g**, the fluorescent signal compared to untreated cells ($n = 10$ and 11 cells for treated vs. untreated). Data points indicate mean and error bars indicate s.e.m. Data were analysed by unpaired Student's *t*-test. $^{*}P < 0.05$, $^{***}P < 0.001$ between treated and untreated groups. **h**, RF treatment of N38 cells expressing anti-GFP–TRPV1/GFP–ferritin significantly increases pCREB levels and **i**, relative *c-fos* (also known as *Fos*) gene expression (measured by quantitative PCR) and these increases are blocked by Ruthenium red (30 and 100 μM). In all cases, columns represent mean and error bars indicate s.e.m. Data were analysed by one way ANOVA with post-hoc Tukey's analysis test. Columns marked with **, #, a or & indicate $P < 0.01$. Each study was repeated on three occasions each with four replicates.

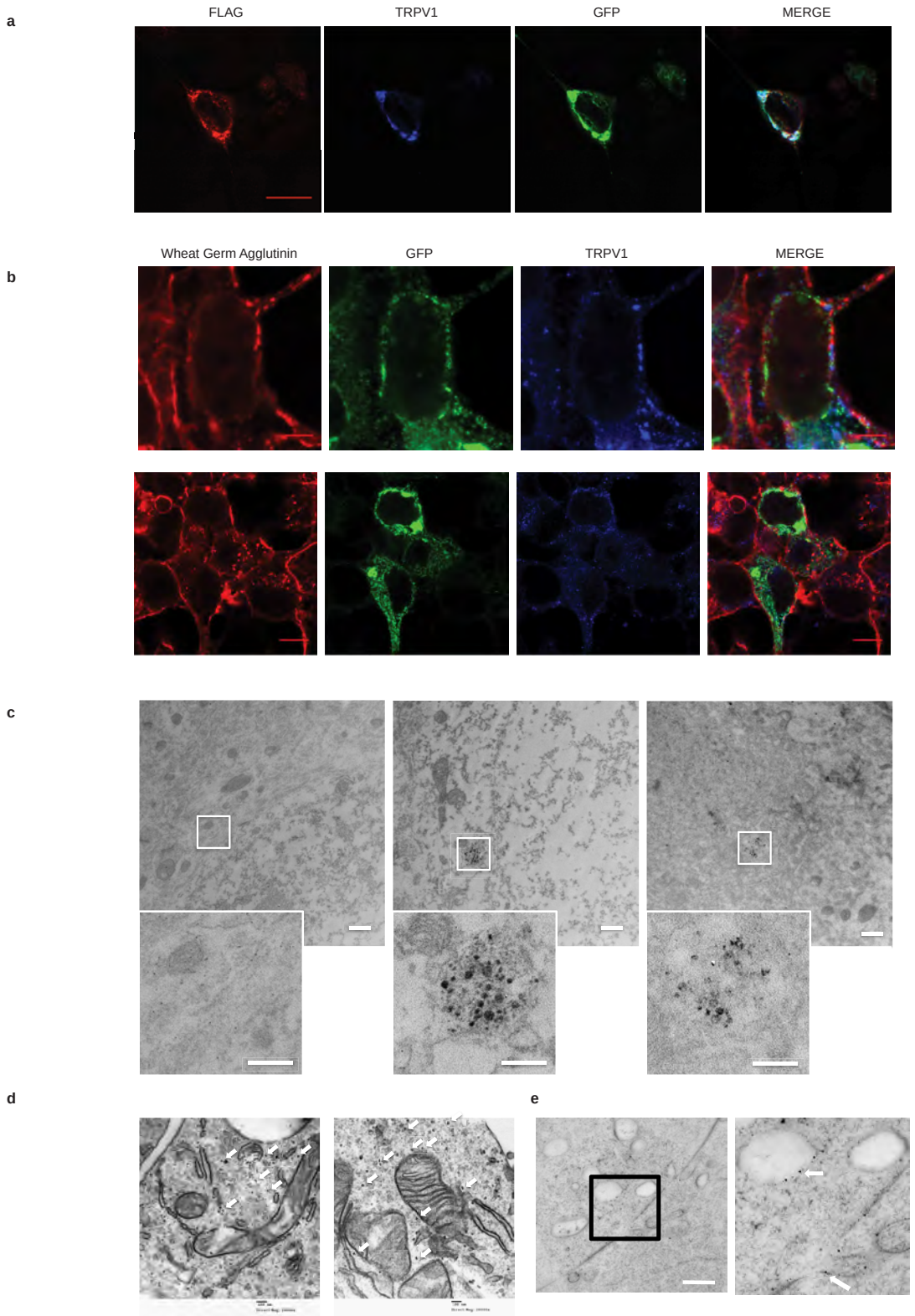

Extended Data Figure 5 | RF treatment of N38 cells *in vitro*. **a**, Immunohistochemistry for Flag-tagged ferritin chimaera (red), TRPV1 (blue) and GFP (green) in N38 cells infected with adenovirus expressing anti-GFP–TRPV1/GFP–ferritin. Scale bar represents 20 μm. **b**, Immunohistochemistry for cell membrane (Alexa-594-conjugated wheat germ agglutinin, red), GFP–ferritin (green) and TRPV1 (blue) in transfected cells showing close proximity of TRPV1 and GFP–ferritin with the cell membrane (upper panels; scale bar, 4 μm) and separate from the cell membrane (lower panels; scale bar, 8 μm). **c**, Immunoelectron microscopy images from hypothalamic sections taken from GK–Cre mice with unilateral expression of anti-GFP–TRPV1/GFP–ferritin showing immunogold-labelled GFP-tagged ferritin (i; centre and right) from the injected side which are absent on the non-injected side (left, scale bar represents 500 nm and 250 nm for magnification). **d**, Electron micrograph of iron-loaded ferritin in HEK cells transfected with ferritin construct alone. **e**, Double immunoelectron microscopy images from stably transfected HEK cells expressing anti-GFP–TRPV1/GFP–ferritin showing co-localization of GFP and TRPV1 at vesicle membranes and at the cell membrane with magnification on the right. Immuno-electron microscopy for GFP and TRPV1 are marked by 5 nm and 12 nm colloidal gold respectively. Scale bar represents 500 nm.

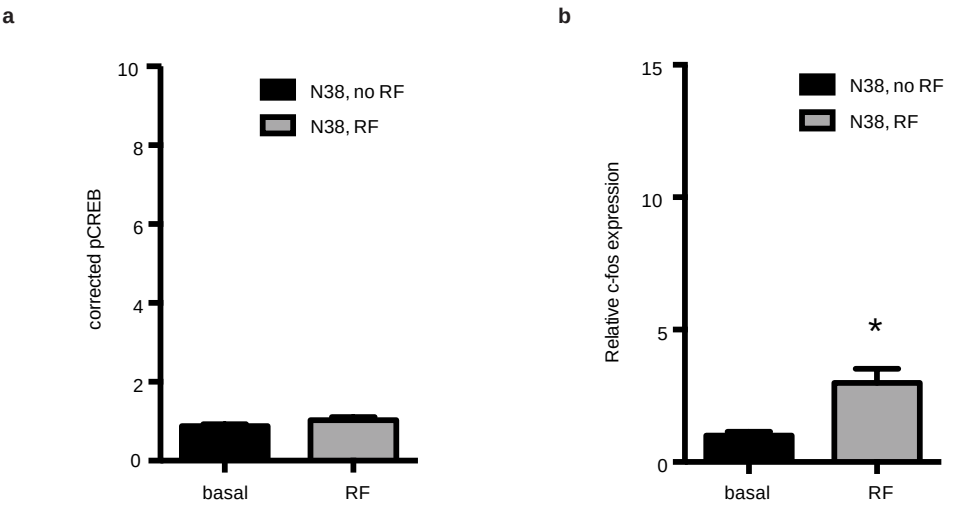

Extended Data Figure 6 | RF treatment of N38 cells *in vitro*. **a**, RF treatment of N38 cells does not alter pCREB levels. In all cases, columns represent mean and error bars indicate s.e.m. Each study was repeated on three occasions each with four replicates. **b**, RF treatment significantly increases relative *c-fos* gene expression. In all cases, columns represent mean and error bars indicate s.e.m. Data were analysed by two-tailed, unpaired Student's *t*-test. $*P < 0.05$. Each study was repeated on three occasions each with four replicates.

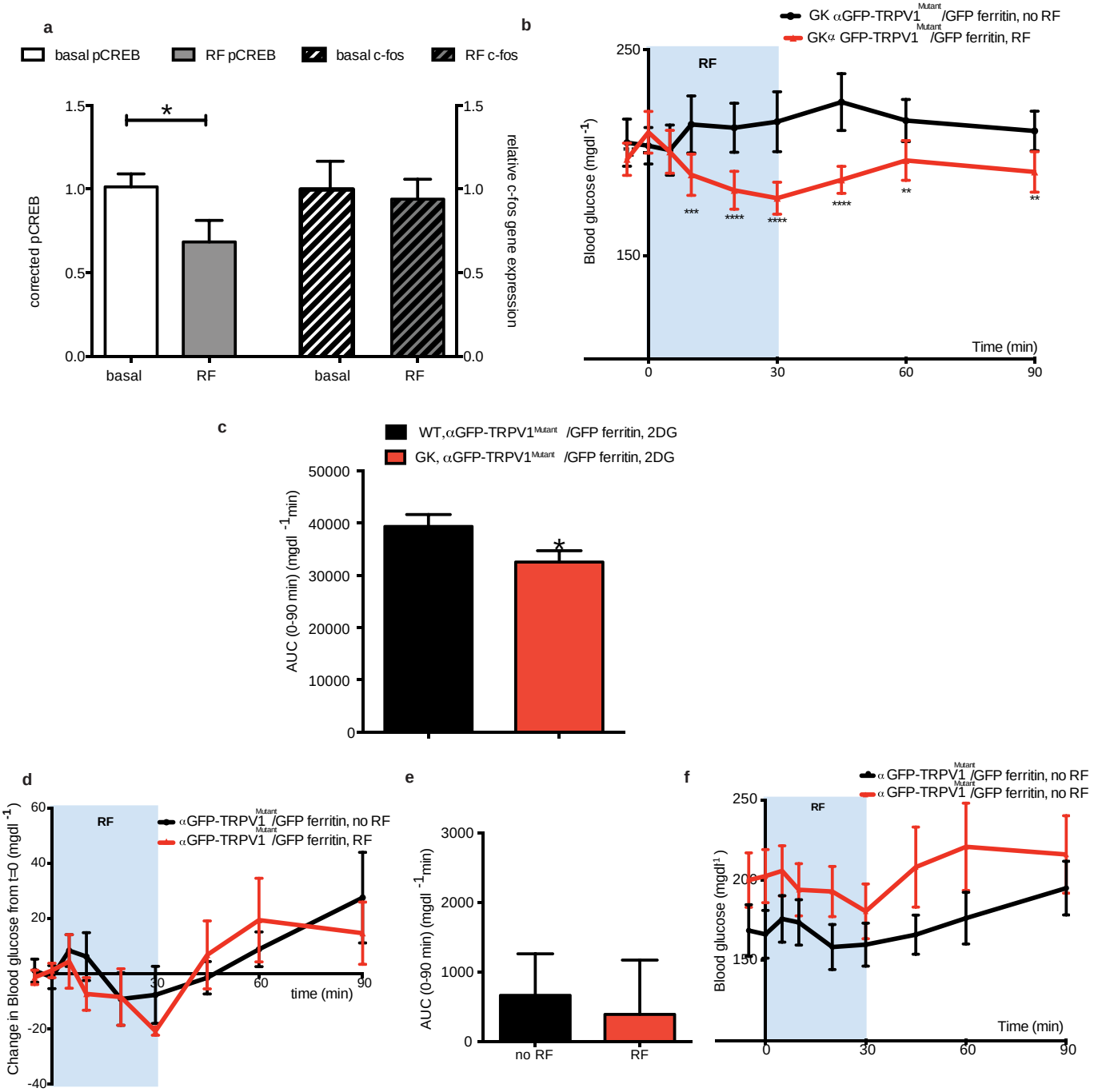

Extended Data Figure 7 | Neural inhibition in GK–Cre and wild-type mice *in vivo*. **a**, Effect of RF treatment of N38 cells expressing anti-GFP–TRPV1^{mutant}/GFP–ferritin on pCREB levels and c-Fos expression. In all cases, columns represent mean and error bars indicate s.e.m. Data were analysed by two-tailed Mann–Whitney *U*-test. $^{*}P < 0.05$. Each study was repeated on three occasions each with four replicates. **b**, RF treatment of GK–Cre mice expressing anti-GFP–TRPV1^{mutant}/GFP–ferritin in the VMH significantly decreases blood glucose compared to no RF treatment ($n = 13$). Data points indicate mean and error bars indicate s.e.m. Data were analysed by two-way ANOVA with Sidak's multiple comparisons. $^{*}P < 0.05$, $^{**}P < 0.01$, $^{***}P < 0.001$, $^{****}P < 0.0001$ between treated and untreated groups. **c**, RF treatment significantly decreases cumulative changes in blood glucose over the course of the study in GK–Cre mice with VMH expression of anti-GFP–TRPV1^{mutant}/GFP–ferritin ($n = 6$) compared to wild-type mice with VMH injection of Ad-FLEX-anti-GFP-TRPV1^{mutant}/GFP-ferritin ($n = 9$) after administration of 2-deoxyglucose to mimic hypoglycaemia. Data are shown as mean and error bars indicate s.e.m. Data were analysed by unpaired Student's *t*-test. $^{*}P < 0.05$. **d**, Effects of RF treatment of wild-type mice injected with anti-GFP–TRPV1^{mutant}/GFP–ferritin in the VMH on changes in blood glucose with time ($n = 8$). Data points indicate mean and error bars indicate s.e.m. Data were analysed by two-way ANOVA with Sidak's multiple comparisons. **e**, Effects of RF treatment of wild-type mice injected with anti-GFP–TRPV1^{mutant}/GFP–ferritin in the VMH on cumulative changes in blood glucose with time ($n = 8$). Data points indicate mean and error bars indicate s.e.m. Data were analysed by two-way ANOVA with Sidak's multiple comparisons. **f**, Effect of RF treatment on blood glucose over the course of the study in wild-type mice with VMH injection of anti-GFP– TRPV1/GFP–ferritin ($n = 8$). Data points represent mean and error bars indicate s.e.m. Data were analysed by two-way ANOVA with Sidak's multiple comparisons.

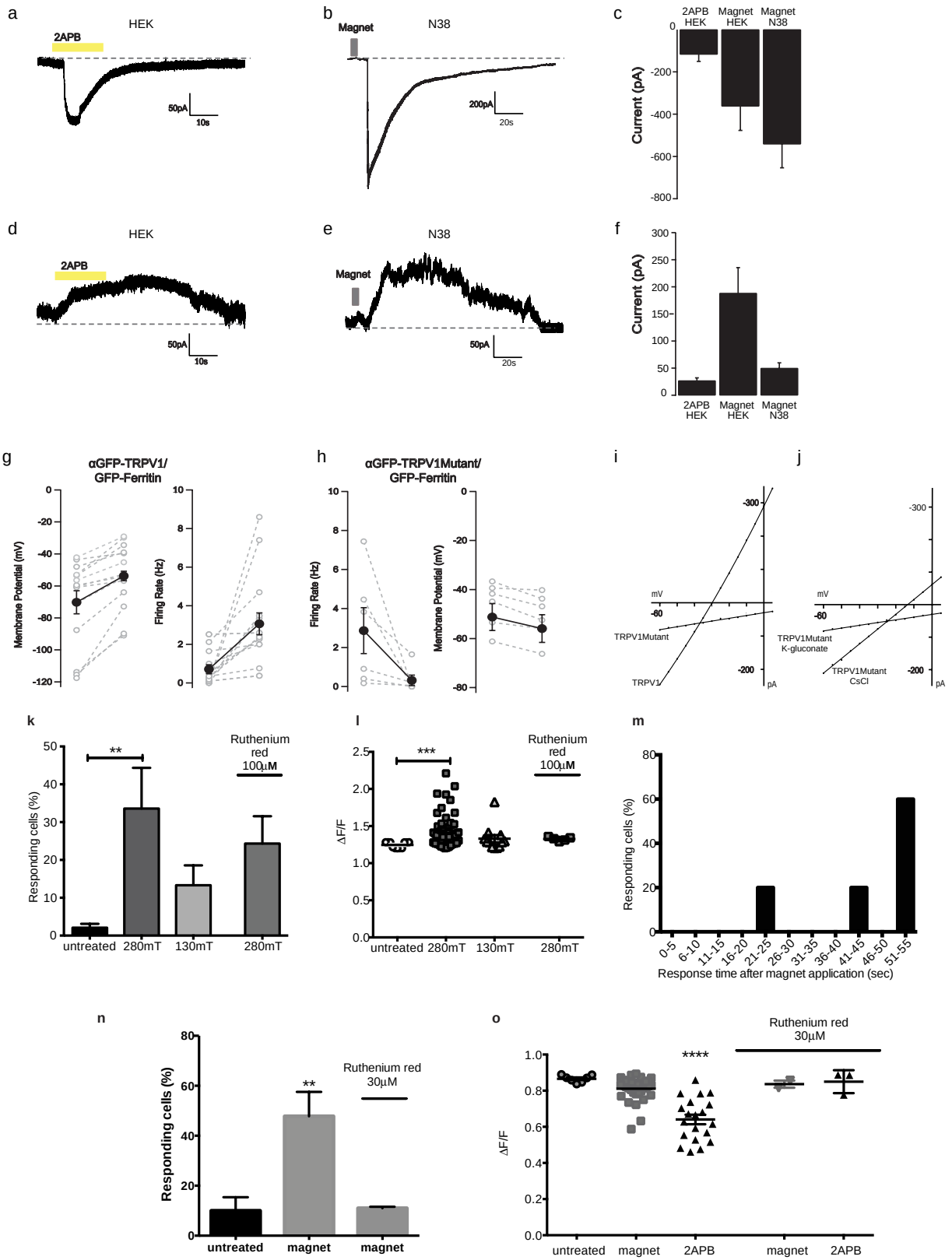

Extended Data Figure 8 | See next page for caption.

Extended Data Figure 8 | Magnetic field activation and inhibition of N38 cells *in vitro*. Electrophysiological recordings of cultured cells. **a**, Current trace from a whole-cell voltage-clamp recording (−60 mV) showing the inward current induced with TRPV1 agonist (2-APB 200 μM) in a HEK cell expressing anti-GFP–TRPV1/GFP–ferritin (representative of four recordings). **b**, Current trace from a whole-cell voltage-clamp recording (−60 mV) induced with a magnetic field (5 s) showing the inward current in stably transfected N38 cells expressing anti-GFP–TRPV1/GFP–ferritin (representative of 15 recordings). **c**, Bar chart summary of mean peak current induced by TRPV1 agonist 2-APB (200 nM, $n = 4$) and magnet activation in cultured cells (HEK, $n = 10$; N38, $n = 15$) expressing anti-GFP–TRPV1/GFP–ferritin. Columns represent mean and error bars indicate s.e.m. Electrophysiological recordings of cultured cells. **d**, Current trace from a whole-cell voltage-clamp recording (−60 mV) showing the outward current induced with TRPV1 agonist (2-APB 200 μM) in a HEK cell expressing anti-GFP–TRPV1^{mutant}/GFP–ferritin (representative of 19 recordings). **e**, Current trace from a whole-cell voltage-clamp recording (−60 mV) induced with a magnetic field (5 s) showing the outward current stably transfected N38 cells expressing anti-GFP–TRPV1^{mutant}/GFP–ferritin (representative of 12 recordings). **f**, Bar chart summary of mean peak current induced by TRPV1 agonist 2-APB (200 nM, $n = 19$) and magnet activation in cultured cells (HEK, $n = 3$; N38, $n = 12$) expressing anti-GFP–TRPV1^{mutant} /GFP–ferritin. Columns represent mean and error bars indicate s.e.m. **g**, Summary data showing magnet-induced changes in membrane potential and firing rate for GK VMH neurons expressing anti-GFP–TRPV1/GFP–ferritin and **h**, anti-GFP–TRPV1^{mutant}/GFP–ferritin. Open circles denote values for individual cells and closed circles denote mean values. Error bars denote s.e.m. For neurons expressing anti-GFP–TRPV1/GFP–ferritin mean membrane potential significantly increased from -70.20 ± 7.246 mV to -53.81 ± 5.349 mV ($n = 14$, $P < 0.0001$, paired t-test). Mean firing rate significantly increased from 0.7084 ± 0.2311 to 3.063 ± 0.5632 ($n = 16$, $P < 0.002$, paired t-test; includes data from 2 cell-attached recordings). For neurons expressing anti-GFP–TRPV1^{mutant}/GFP–ferritin mean membrane potential significantly decreased from -51.2 ± 5.519 mV to -55.93 ± 5.636 mV ($n = 6$, $P = 0.03$; Wilcoxon matched pairs). Mean firing rate significantly decreased from 2.868 ± 1.177 to 0.3167 ± 0.2685 ($n = 6$, $P = 0.03$; Wilcoxon matched pairs). Current–voltage relationship of 2-APB-activated TRPV1^{mutant} channels shows limited cation permeability and increased chloride permeability. **i**, Limited conductance of TRPV1^{mutant} channels compared to wild-type when the predominant internal ions are K^+ and gluconate. **j**, Conductance is increased for anti-GFP–TRPV1^{mutant} channels when the predominant internal ions are Cs and Cl (isometrical chloride). **k**, Calcium imaging in stably transfected N38 cells expressing anti-GFP–TRPV1/GFP–ferritin demonstrates a magnetic field-strength-dependent increase in the percentage of responding cells (>20% increase in fluorescence) ($n = 7$, 10, 3 imaging studies, respectively) and **l**, the fluorescent signal compared to untreated cells ($n = 11$, 48, 12 cells, respectively). The effects of magnet stimulation were blocked by Ruthenium red. Data points indicate mean and error bars indicate s.e.m. Data were analysed by two-way ANOVA with Sidak's multiple comparisons. $^*P < 0.05$, $^{**}P < 0.01$, $^{***}P < 0.001$ $^{****}P < 0.0001$ between treated and untreated groups. **m**, Histogram representing the response time (to reach 20% increase in fluorescence) in magnet-treated N38 cells expressing anti-GFP–TRPV1/GFP–ferritin ($n = 68$ cells). **n**, Treatment of N38 cells expressing anti-GFP–TRPV1^{mutant}/GFP–ferritin with magnet ($n = 6$ occasions) significantly increased the percentage of responding cells (i) (>10% decrease in chloride indicator, MQAE,fluorescence) compared to untreated cells ($n = 4$ occasions) and **o**, the reduction in MQAE signal. Ruthenium red reduced both the percentage of responding cells and the magnitude of the response ($n = 2$ occasions). In all cases, columns represent mean and error bars indicate s.e.m. Data were analysed by Kruskal–Wallis test with Dunn's multiple comparison test. Columns marked with $^{**}P < 0.01$ vs. untreated, columns marked with $^{****}P < 0.001$ vs. untreated.

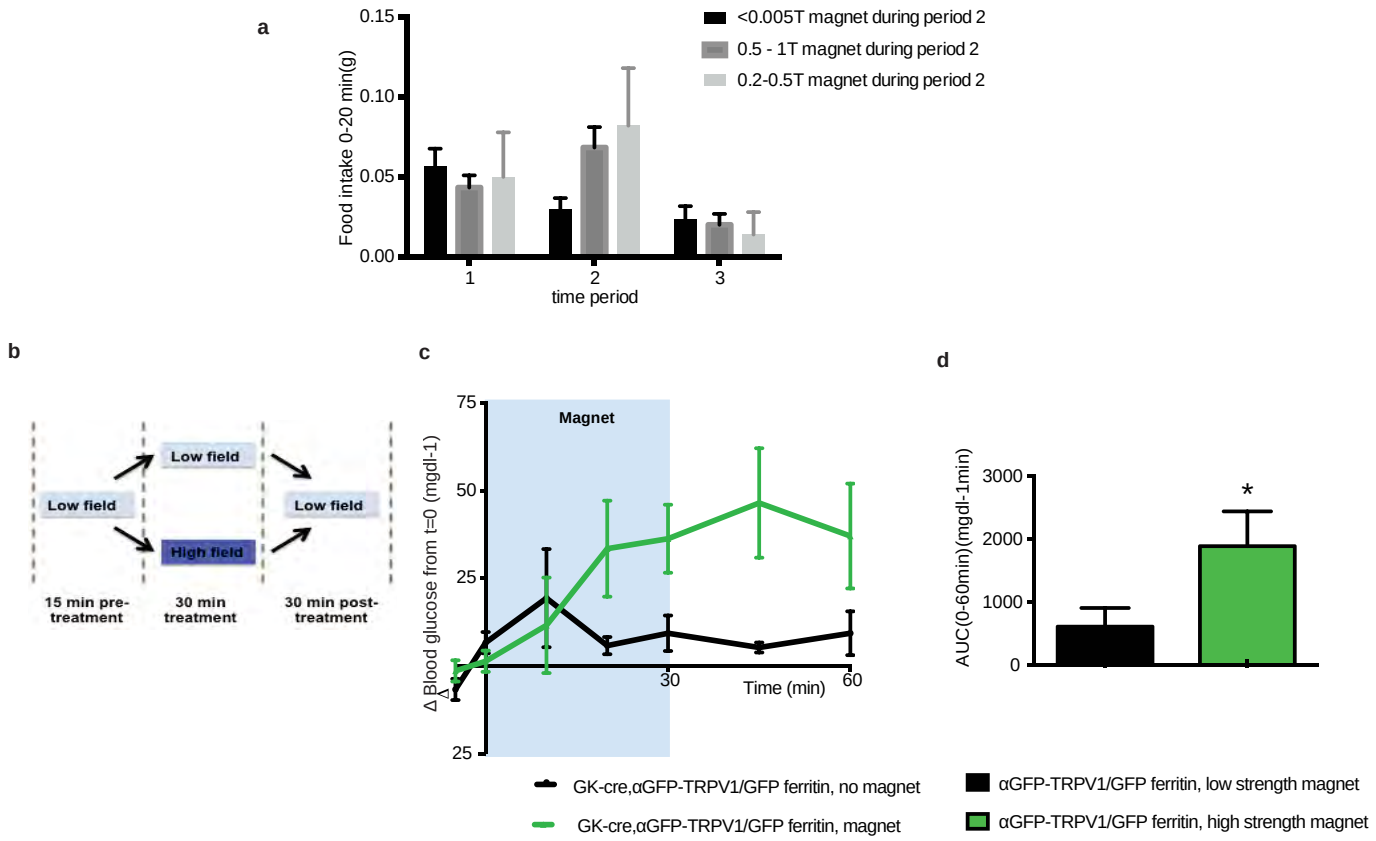

Extended Data Figure 9 | Non-invasive neural activation *in vivo* using a static magnetic field. a, The effect of moderate (0.2–0.5 T) magnetic field strength on food intake in GK–Cre mice expressing anti-GFP–TRPV1/GFP–ferritin in the VMH ($n = 5$). Columns represent mean and error bars indicate s.e.m. **b**, Schema of the crossover protocol used to examine the effect of neural activation with a static magnetic field on blood glucose. **c**, Magnetic field treatment of GK–Cre mice following VMH injection of anti-GFP–TRPV1/GFP–ferritin significantly increases blood glucose compared to no magnet treatment ($n = 6$). Data points indicate mean and error bars indicate s.e.m. Data were analysed by two-way ANOVA with Sidak's multiple comparisons. **d**, Magnet treatment significantly increases cumulative change in blood glucose over the course of the study in GK–Cre mice with VMH injection of anti-GFP–TRPV1/GFP–ferritin ($n = 6$) compared to the same mice without magnet treatment. In all cases, columns represent mean and error bars indicate s.e.m. Data were analysed by Wilcoxon matched pairs signed rank test. $^*P < 0.05$. **e**, Effects of static magnetic field treatment of wild-type mice with VMH injection of anti-GFP–TRPV1/GFP–ferritin on changes in blood glucose with time ($n = 6$). Data points indicate mean and error bars indicate s.e.m. Data were analysed by two-way ANOVA with Sidak's multiple comparisons. **f**, Effects of static magnetic field treatment of wild-type mice injected with anti-GFP–TRPV1/GFP–ferritin in the VMH on food intake ($n = 6$). Data points indicate mean and error bars indicate s.e.m. Data were analysed by two-way ANOVA with Sidak's multiple comparisons.

a

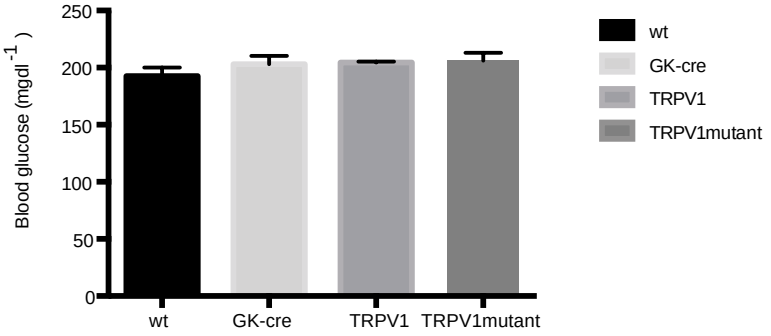

b

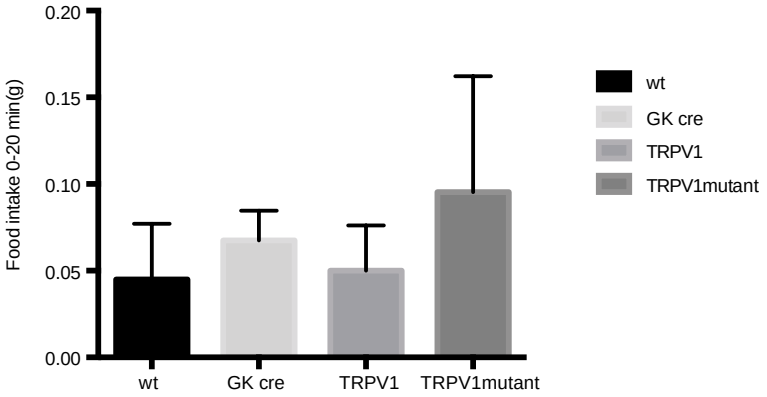

Extended Data Figure 10 | Baseline characteristics in mice expressing anti-GFP–TRPV1/GFP–ferritin or anti-GFP–TRPV1^{mutant}/GFP–ferritin. a, Non-fasting blood glucose did not differ significantly between wild-type, GK–Cre and GK–Cre mice injected with anti-GFP–TRPV1/GFP–ferritin or anti-GFP–TRPV1^{mutant}/GFP–ferritin ($n = 10$, 8, 8 and 5, respectively). Columns represent mean and error bars indicate s.e.m. **b**, Food intake following a 4 h fast did not differ significantly between wild-type, GK–Cre and GK–Cre mice injected with anti-GFP–TRPV1/GFP–ferritin or anti-GFP–TRPV1^{mutant}/GFP–ferritin ($n = 6$, 4, 6 and 13 respectively). $^{*}P < 0.05$. Columns represent mean and error bars indicate s.e.m.